NASA

National Aeronautics and
Space Administration

STUDY OF VAPOR FLOW INTO A CAPILLARY ACQUISITION DEVICE

By

Franklin T. Dodge
Edgar B. Bowles

Southwest Research Institute
San Antonio, Texas

Prepared For

SOUTHWEST RESEARCH INSTITUTE
SAN ANTONIO   HOUSTON

STUDY OF VAPOR FLOW INTO A
CAPILLARY ACQUISITION DEVICE

By

Franklin T. Dodge
Edgar B. Bowles

Southwest Research Institute
San Antonio, Texas

Prepared For

N82- 24452#

1. Report No. NASA-CR-167883	2. Government Accession No.	3. Recipient's Catalog No.
4. Title and Subtitle Study of Vapor Flow Into a Capillary Acquisition Device		5. Report Date April 1982
		6. Performing Organization Code
7. Author(s) Franklin T. Dodge Edgar B. Bowles		8. Performing Organization Report No. Final Report, 02-6369
		10. Work Unit No.
9. Performing Organization Name and Address Southwest Research Institute 6220 Culebra Rd San Antonio, Texas 78284		11. Contract or Grant No. NAS3-22664
		13. Type of Report and Period Covered Contractor Report
12. Sponsoring Agency Name and Address National Aeronautics and Space Administration Washington, D. C. 20546		14. Sponsoring Agency Code

15. Supplementary Notes

Project Manager, E. P. Symons, Propulsion and Power Division,
NASA Lewis Research Center, Cleveland, Ohio 44135

16. Abstract

An analytical model was developed that prescribes the conditions for vapor flow through the window screen of a start basket. Several original sub-models were developed as part of this model. The sub-models interrelate such phenomena as the effect of internal evaporation of the liquid, the bubble-point change of a screen in the presence of wicking, the conditions for drying out of a screen through a combination of evaporation and pressure difference, the vapor inflow rate across a wet screen as a function of pressure difference, and the effect on wicking of a difference between the static pressure of the liquid reservoir and the surrounding vapor. Most of these interrelations were verified by a series of separate-effects tests, which were also used to determine certain empirical constants in the models. The equations of the model were solved numerically for typical start-basket designs, and a simplified start basket was constructed to verify the predictions, using both volatile and non-volatile test liquids. The rest results verified the trends predicted by the model. A further series of separate-effects tests is recommended to complete the development of the model.

17. Key Words (Suggested by Author(s)) Start Basket, Window Screen, Vapor Inflow, Propellant Control, Screen Acquisition Systems, Fluid Mechanics, Evaporation	18. Distribution Statement Unclassified - Unlimited		
19. Security Classif. (of this report) Unclassified	20. Security Classif. (of this page) Unclassified	21. No. of Pages 118 + prelims + dist. list	22. Price*

This Page Intentionally Left Blank

TABLE OF CONTENTS

LIST OF FIGURES

LIST OF TABLES

iv

ABSTRACT

An analytical model was developed that prescribes the conditions for vapor flow through the window screen of a start basket. Several original sub-models were developed as part of this model. The sub-models interrelate such phenomena as the effect of internal evaporation of the liquid, the bubble-point change of a screen in the presence of wicking, the conditions for drying out of a screen through a combination of evaporation and pressure difference, the vapor inflow rate across a wet screen as a function of pressure difference, and the effect on wicking of a difference between the static pressure of the liquid reservoir and the surrounding vapor. Most of these interrelations were verified by a series of separate-effects tests, which were also used to determine certain empirical constants in the models. The equations of the model were solved numerically for typical start-basket designs, and a simplified start basket was constructed to verify the predictions, using both volatile and non-volatile test liquids. The test results verified the trends predicted by the model. A further series of separate-effects tests is recommended to complete the development of the model.

1. INTRODUCTION

Spacecraft that require restarting of their liquid propellant engines must have the propellants positioned over the engine inlets even after adverse disturbances. The use of fine-mesh wire screens to assure this by forming a passive capillary acquisition system was introduced in the early 1960's in the Agena upper stage vehicle (Ref. 1). Since then, a general class of capillary devices called "start baskets" has been used successfully in many applications where the propellants are storable (that is, remain liquid). For cryogenic propellants, however, unavoidable heat transfer may cause local boiling and thereby drive liquid out of the basket or let vapor in. The effectiveness of the baskets would thereby be diminished. There has, as a result, been much research aimed at characterizing and understanding capillary acquisition systems for cryogenic propellants; Refs. 2-5 are typical examples.

Incorporating a "window" screen in the start basket design to control vapor inflow has been advanced as one promising way of overcoming the unfavorable effects of cryogenic propellant boiling. An extensive experimental program meant to quantify the behavior of such designs, and specifically the response of the window screen, has been conducted previously (Ref. 2). These tests were only partially successful because of a lack of repeatability from test to test. In particular, for a start basket of relatively small size, short periods of vapor inflow were followed by longer periods when the window screen apparently remained sealed, whereas for larger baskets the inflow was more or less steady. The reasons for such differences were not apparent.

Thus, a number of questions still remain about the way the window screen, the main screens, and the vapor and liquid flows interact. The research presented in this report was designed to answer such questions. First, analytical models were formulated that describe the response of the various parts of a start basket; previous work as well as new results were used to develop these models. The separate models were then assembled into an overall predictive model which was solved by numerical integration. Next, a

series of "separate-effects" tests were conducted to evaluate one-at-a-time the analytical models and to determine certain empirical constants. Finally, a simplified start basket was constructed and tested, and the test results were compared to the predictions of the analytical model.

2. ANALYTICAL MODELS

The analytical models are developed with the aid of the simplified start basket sketched in Figure 1. To enhance their generality, they are formulated first in terms of specified flow rates and pressure balances. The flows are then related to the pressures, with functional forms assumed on the basis of physical reasoning when available data or analyses are lacking.

2.1 Response of Vapor Space

As liquid evaporates from the external surfaces of the main screens, liquid is drawn out of the main liquid volume in order to keep the channels full. (The capillary-induced suction at the top of the channels provides the driving force for the flow.) This withdrawal creates a vapor volume. To simplify the analysis, it is assumed that gravity or a gravity-like acceleration is directed perpendicularly to the window screen surface; thus, the vapor volume will be below the window screen and in contact with it. (Other configurations could also be analyzed, but this one corresponds to most ground-based tests.) The vapor is treated as an ideal gas, and the molecular weight of the gas flowing into the vapor space across the screen is assumed not to be greatly different from the vapor. The pressure change in the vapor space is therefore:

$$\frac{dP}{dt} = -\frac{P}{V}\left(\frac{dV}{dt}\right) + \frac{RT}{V}(\dot{m}_e A_{vs} + \dot{M}_v) \tag{1}$$

(Symbols are defined in the Appendix; many are also shown in Figure 1.)

The rate of increase of the vapor volume and the corresponding change of the liquid level are given by:

$$\frac{dV}{dt} = (\dot{m}_o A_o + \dot{m}_e A_{vs})/\rho_L \tag{2}$$

$$A_i \frac{dh}{dt} = \frac{dV}{dt} \tag{3}$$

4
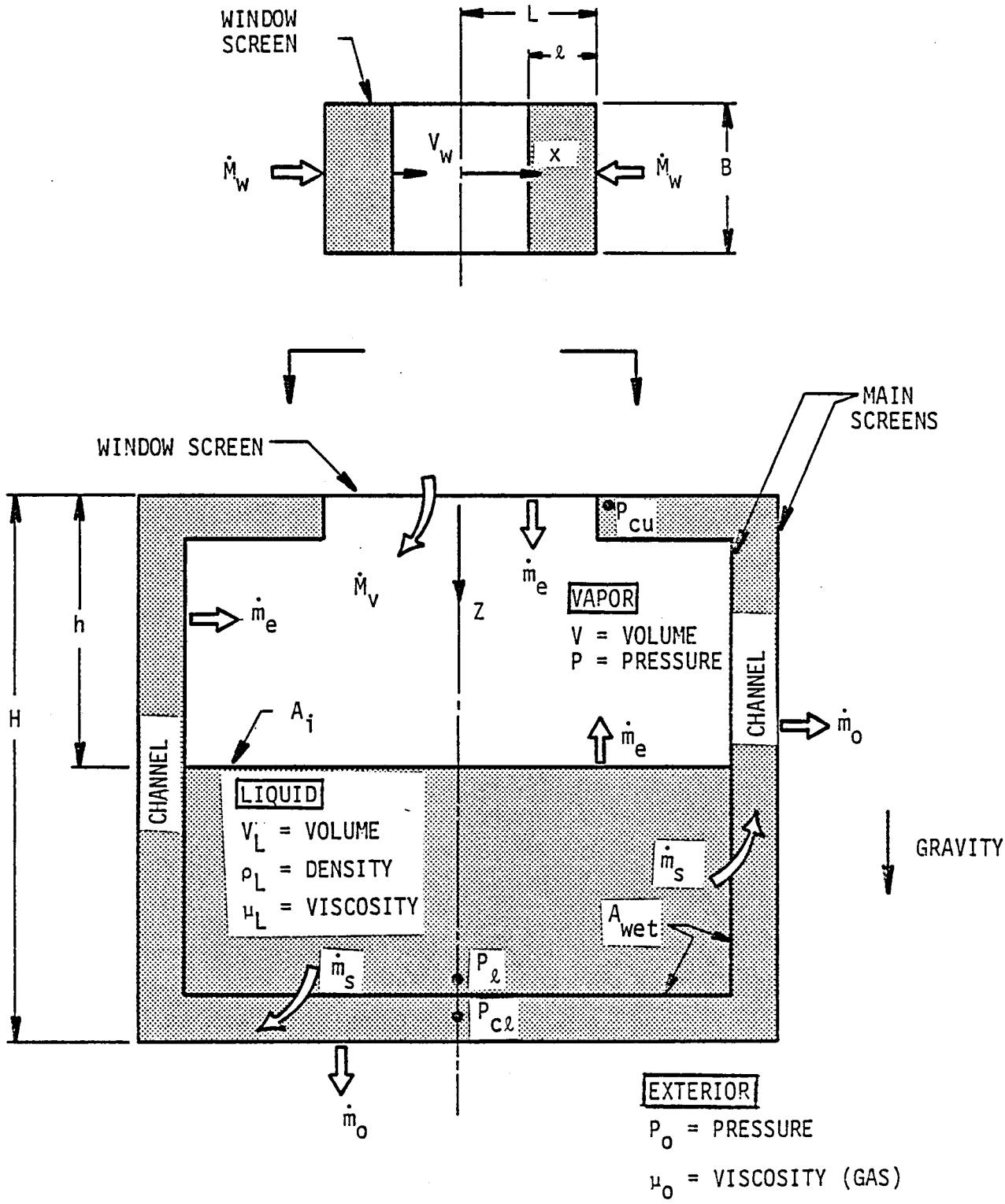
FIGURE 1. NOMENCLATURE FOR ANALYSIS OF START BASKET

Here, A_i is the interfacial area between the liquid and the vapor; in general, A_i will vary with h as a function of the shape of the start basket, but in this analysis it is assumed to be constant.

The internal and external evaporation rates and the flow through the window screen will be correlated with more fundamental parameters later.

2.2   Pressure and Flow in Channel

The flow from the main liquid volume into the channels occurs at the locations where the internal surfaces of the main screens are wet on both sides. The relation between the pressure differential and the flow across a screen has been determined previously by several investigators (Refs. 6 and 7, for example). For the low-speed flows of interest here, only the "viscous" part of the correlations must be included; thus

$$\dot{m}_s(x,z)/\rho_L = [P_L(x,z) - P_c(x,z)]/\mu_L a_{ms} F_{ms} \tag{4}$$

where F_{ms} is a resistance parameter that is a combination of geometric factors that describe the weave of the screen, and a_s is an experimentally-determined factor. In terms of these factors, F_{ms} is

$$F_{ms} = (bA_r^2 Q/V_r^2)_{ms} \tag{5}$$

The subscript "ms" implies that the relevant factors for the main screen must be used in determining F_{ms}; likewise, "ws" would imply that the window screen resistance is meant.

In comparison to the pressure differential across the screen, the pressure change along the channel caused by viscous friction and momentum effects is negligible. Consequently, the pressure differential is not a function of position and is everywhere equal to $P_\ell - P_{c\ell}$. Thus, Equation (4) can be integrated over the wetted surface to compute the total flow into the channels. Since the result is equal to the total evaporation rate, the pressure at the bottom of the channel determined in terms of the evaporative flows is:

$$P_{c\ell} = P_\ell - (\dot{m}_o A_o + \dot{m}_e A_{vs}) \mu_L a_{ms} F_{ms} / A_{wet} \tag{6}$$

The static pressures in the channels, the main liquid volume, and the vapor space can be expressed as:

$$P_{cu} = P_{c\ell} - \rho_L g H \tag{7}$$

$$P_\ell = P + \Delta P_{\ell v} + \rho_L g(H - h) \tag{8}$$

$$P = P_o - \Delta P_{ov} \tag{9}$$

Here, $\Delta P_{\ell v}$ is the pressure difference (if any) between the surface of the main liquid and the enclosed vapor, and ΔP_{ov} is the difference between the exterior pressure and the vapor. The pressure difference ΔP_{ov} will later be related to the bubble-point pressure of the window screen, the wicking flow, and similar quantities. For a storable liquid (that is, one carried at temperatures well below its boiling point), $\Delta P_{\ell v}$ will be negligibly small; on the other hand, for a cryogenic liquid or other near-boiling liquid, the liquid surface will be at the thermodynamic saturation point, and $\Delta P_{\ell v} = P_{sat} - P$, where the saturation pressure is a specified function of the temperature.

It will be convenient later to have P_{cu} expressed directly in terms of the observable liquid level and the vapor space pressure. Combining Equations (7), (8), and (9) gives:

$$P_{cu} = P_o - (\Delta P_{ov} - \Delta P_{\ell v}) - \rho_L g h -$$

$$(\dot{m}_o A_o + \dot{m}_e A_{vs}) \mu_L a_{ms} F_{ms} / A_{wet} = P_o - \Delta P_{oms} \tag{10}$$

2.3 Wicking Along Window Screen

As liquid evaporates from the window screen, it must be replaced by wicking from the liquid in the channels. Wicking is due to capillarity, and the analysis of it given here follows that presented in Ref. 8. The

capillary pressure in the liquid at the liquid-vapor interface across the screen thickness, P_σ, is a function of the liquid surface tension σ and the screen weave geometry. Letting the wicking velocity $v_w = d\ell/dt$, the correlation given in Ref. 8 can be expressed in terms of the capillary pressure as

$$P_{cu} - P_\sigma = C_{ws}\mu_L \ell (d\ell/dt)/b_{ws}^2 \tag{11}$$

Here, C_{ws} is a non-dimensional wicking resistance factor that must be determined experimentally for each screen type. Equation (11) simply represents the viscous pressure drop along a channel of length ℓ and height b_{ws}; the parameter C_{ws} accounts for the effects of screen weave (that is, for the fact that the actual channel height is not b_{ws}). Wicking in only one-dimension is assumed in Equation (11), but the generalization to two-dimensions is not difficult. Equation (11) can be rearranged to predict the wicking velocity:

$$\frac{d\ell}{dt} = (P_{cu} - P_\sigma)b_{ws}^2/C_{ws}\mu_L \ell \tag{12}$$

In most previous analyses of wicking (for example, Refs. 2 and 8), it has been tacitly assumed that the wicking reservoir and the screen are both exposed to the same environmental pressure (for example, the atmosphere) or, more exactly, that any difference in the two environmental pressures has no effect. In that case, the capillary pressure is always less than the reservoir pressure, and

$$P_{cu} - P_\sigma = \phi_{ws}\sigma/D_{pws} \tag{13}$$

D_{pws} is the bubble-point diameter of the window screen and ϕ_{ws} is an experimentally-determined parameter defined here that relates the wicking "pore" diameter to the bubble-point diameter. Equation (12) can then be integrated to give

$$\ell^2 = 2\left(\frac{\phi b^2}{D_p C}\right)_{ws} \left(\frac{\sigma t}{\mu_L}\right) \tag{14}$$

By measuring the wicking length as a function of time, the combined parameter $(\phi/C)_{ws}$ can be determined. Either ϕ or C must be determined separately by other kinds of tests, as described later. (Values of $\phi b^2/CD_p$ for many screens are given in Ref. 8).

When the screen and the reservoir are exposed to different static pressures, it is not legitimate to use Equation (14). For that case, the analogy between wicking in a screen and the capillary-induced flow in a rigid-walled tube is invalid. For a tube connected to a reservoir, the liquid pressure in the tube "floats" with the pressure in the reservoir, and the capillary suction at the open end of the tube is superimposed on whatever pressure exists in the liquid in the tube. But for a screen, the walls of the tube are not rigid or impermeable; in fact, there are no real walls. The reservoir pressure cannot be communicated to the fluid in the "tube", except in the very near vicinity of the reservoir, since the permeable walls of the tube are exposed to a different surrounding pressure. It is proposed here to model wicking under these conditions by expressing both P_σ and P_{cu} in terms of the same reference pressure, say, the exterior pressure. The curvature of the liquid interface in the wicking screen still creates a wicking suction relative to the surrounding pressure but P_σ must now be written as

$$P_\sigma = P_o - \phi_{ws}\sigma/D_{pws} \qquad (15)$$

(Further, in an application to a wet window screen, the static pressure may be different on either side of the screen. The liquid-vapor interface curvature on the two lateral surfaces must therefore be different, rather than the same as is the case when there is no pressure difference. Consequently, the wicking surface curvature and wicking pressure may also be different than $\phi\sigma/D_p$. More will be said about this later.) From Equation (10), the wicking reservoir pressure is $P_{cu} = P_o - \Delta P_{oms}$, so Equation (11) should be rewritten now as:

$$\frac{\phi_{ws}\sigma}{D_{pws}} - \Delta P_{oms} = C_{ws}\mu_L \ell \, (d\ell/dt)/b_{ws}^2 \qquad (16)$$

Note that the decrease in the reservoir pressure with respect to the exterior pressure that acts on the window screen diminishes the ability of the screen to wick.

To account for the change in ϕ_{ws} when there is a pressure difference across the screen as mentioned above, it is proposed here to model the capillary suction pressure decrease as a linear function of ΔP_{ov}:

$$\frac{d\phi_{ws}}{d\Delta P_{ov}} = -K_1 \bar{\phi}_{ws}/(4\sigma/D_{pws}) \qquad (17)$$

K_1 is a non-dimensional parameter defined here that must be determined experimentally as a function of screen weave, $\bar{\phi}_{ws}$ is the value of ϕ_{ws} for $\Delta P_{ov} = 0$ (and is a property of the screen), and $4\sigma/D_{pws}$ is the normal bubble-point pressure. The integrated form of Equation (17) will be given later, when the allowable limits on ΔP_{ov} have been determined. Equation (17) expresses the fact that a part of the capillary potential of the screen is used to support ΔP_{ov} and, thus, the full wicking potential cannot be realized.

When the window screen loses liquid by evaporation, the wicking velocity in the above equations depends on the evaporation rate:

$$\frac{dv_w}{dx} = \dot{m}_w/\rho_L b_{fws} \qquad (18)$$

Here, $\dot{m}_w$ is the evaporation rate per unit area from both surfaces of the screen, and b_{fws} is an effective open thickness of the screen; the product Bb_{fws} is the actual cross-sectional flow area of the screen occupied by liquid. Conceptually, b_{fws} can be related to b_{ws}, the true screen thickness, by imagining it to be the width of a flow channel. Then, Equation (11) could be written as

$$P_{cu} - P_\sigma = 12\mu_L \ell(d\ell/dt)/b_{fws}^2 \qquad (19)$$

so that

$$b_{fws} = b_{ws}/(C_{ws}/12)^{1/2} \qquad (20)$$

For accuracy, b_{fws} should be determined experimentally as described later, but experimental determinations should give results of the same order of magnitude as Equation (20).

Equation (18) and the differential form of Equation (16) are used to predict the wicking response of the window screen. Expressing $(\phi_{ws}\sigma/D_{pws} - \Delta P_{oms})/\ell$ as dP_W/dx gives, after some manipulation:

$$\frac{d^2 P_W}{dx^2} = \frac{C_{ws}\mu_L}{b_{ws}^2}\left(\frac{dv_s}{dx}\right) = \frac{C_{ws}\mu_L \dot{m}_w}{\rho_L b_{ws}^2 b_{fws}} \tag{21}$$

The boundary conditions for Equation (21) are

$$\frac{dP_W}{dx} = 0 \text{ at } x = L - \ell \tag{22}$$

(for otherwise v_s is not zero at the dry-out location) and

$$P_W = P_{cu} - F_j \mu_L v_w \text{ at } x = L \tag{23}$$

where F_j is the concentrated resistance (with dimensions of reciprocal length) of the junction at the window and the main screen. For a well-manufactured junction, F_j is probably near zero, but it is retained here for generality. The wicking velocity at $x = L$ is $\dot{m}_w\ell/\rho_L b_{fws}$, so the result of integrating Equation (21) is

$$P_W(x) = P_0 - \Delta P_{oms} - \frac{\mu_L \ell^2 \dot{m}_w}{2\rho_L b_{ws}^2 b_{fws}} \left\{ C_{ws}\left[1 - \left(\frac{x}{\ell} - \frac{L}{\ell} + 1\right)^2\right] \right.$$
$$\left. + \frac{2F_j b_{ws}^2}{\ell} \right\} \tag{24}$$

The primary use of Equation (24) is to determine the maximum rate of evaporation from the window screen that can be sustained for any given wicking length ℓ. At $x = L - \ell$, P_{ws} is just the maximum wicking suction that is available; that is, it is $P_0 - \phi_{ws}\sigma/D_{pws}$. The wetted length, ℓ, of the window screen is therefore the solution of Equation (24) for $x = L - \ell$; that is:

$$\ell^2 + 2\ell \left(\frac{F_j b_{ws}^2}{C_{ws}}\right) - \frac{2\rho_L b_{ws}^2 b_{fws}}{\mu_L \dot{m}_w C_{ws}} \left(\frac{\phi_{ws}\sigma}{D_{pws}} - \Delta P_{oms}\right) = 0 \tag{25}$$

If $\ell \geq L$, the screen remains wet completely to the center; otherwise, the area $2B(L - \ell)$ will dry out.

2.4 Bubble-Point of Window Screen

Instead of drying out in accordance with Equation (25), the window screen can admit vapor simply because $P_o - P = \Delta P_{ov}$ exceeds the bubble-point pressure. Again, it must be realized that the interfacial curvatures of the liquid at the screen surfaces and the bubble-point pressure will be different in the presence of wicking, since part of the available capillary potential is used to support the wicking. A linear decrease is proposed here:

$$(\Delta P_{ov})_{max} = \frac{4\sigma}{D_{pws}} \left\{1 - K_2 \left[\frac{\Delta P_w}{(\phi\sigma/D_p)_{ws}}\right]\right\} \tag{26}$$

where K_2 is an experimentally-determined parameter defined here, ΔP_w is the actual wicking pressure difference along the screen, and $\bar{\phi}_{ws}\sigma/D_{pws}$ is the maximum possible wicking pressure difference. (Both pressures can be expressed per unit of wicking length by dividing by ℓ.) Since ΔP_{ws} can be related to the evaporation from the screen and $\bar{\phi}_{ws}\sigma/D_{pws}$ related to the maximum possible evaporation rate, a more useful form of Equation (26) is

$$(\Delta P_{ov})_{max} = \frac{4\sigma}{D_{pws}} [1 - K_2 \dot{m}_w/(\dot{m}_w)_{max}] \tag{27}$$

The maximum possible evaporation rate per unit area, which is a function of the wicking length as well as the screen weave and liquid properties, is found from Equation (25) by setting $\ell = L$. The parameters F_j and ΔP_{oms} are neglected since they depend on the design of the start basket and are not related to the properties of the window screen. Thus,

$$(\dot{m}_w)_{max} = \frac{2b_{ws}^2 b_{fws}}{L^2 C_{ws}} \left(\frac{\rho_L \bar{\phi}_{ws}\sigma}{\mu_L D_{pws}}\right) \tag{28}$$

(This incidentally shows the proportionality between the evaporation rate and the wicking pressure mentioned above.) Equation (28) agrees with the analysis presented in Ref. 8. By inserting Equation (28) into Equation (27), the bubble-point decrease can be expressed in terms of screen and liquid parameters:

$$(\Delta P_{ov})_{max} = \frac{4\sigma}{D_{pws}} [1 - K_2(\frac{\dot{m}_w \mu_L D_{pws} L^2 C_{ws}}{2\rho_L \phi_{ws} \sigma b_{ws}^2 b_{fws}})] \qquad (29)$$

A somewhat analogous effect of evaporation on bubble-point has been reported in Ref. 9. There it was found that the bubble-point slowly decreased as liquid evaporated from an initially wet screen when the liquid was not replenished by wicking. When about half of the liquid had evaporated, the bubble-point decreased rapidly to zero. This is an unsteady phenomenon, as contrasted to the steady state decrease expressed by Equation (29), but a similar behavior might occur in start baskets during ground testing, as will be discussed later.

Previous tests (Ref. 10) have shown moreover that, after the bubble-point pressure of a screen has been exceeded, the pressure differential must be reduced to values well below the bubble-point in order to make the screen re-seal. While this hysteresis effect has been demonstrated only for screens covered on one side by a thin layer of liquid (as in the usual kind of bubble-point test), it is assumed here that the same behavior would occur for a screen that is merely thoroughly wet. Thus, the resistance of the screen to a pressure differential is given by:

$$\Delta P_{ov} = P_o - P \geq (\Delta P_{ov})_{max} \qquad (30)$$

to initiate an inflow after which:

$$\Delta P_{ov} = \leq K_3 (\Delta P_{ov})_{max} \qquad (31)$$

to cause resealing. From the data of Ref. 10, it appears that $K_3 \approx 0.57$.

The decrease of bubble-point as a function of wicking and the decrease of wicking as a function of pressure differential are evidently related. In fact, since $d\phi_{ws}/d\Delta P_{ov} = 1/[dp_{ov}/d\phi_{ws}]$, it can be shown by manipulating Equation (17) and Equation (26) with $\Delta P_w = \phi\sigma/D_{pws}$ that $K_1 = 1/K_2$. Equation (26) can be used to determine the limits of integration for Equation (17). As long as a screen remains completely wet, its bubble-point will be greater than zero even if $\dot{m}_w = (\dot{m}_w)_{max}$. Thus, $K_2 < 1$, and from Equation (26) or (27) it can be concluded that ΔP_{ov} decreases from $4\sigma/D_{pws}$ to $(4\sigma/D_{pws})(1 - K_2)$ as the wicking (or evaporation) increases from zero to its maximum. That implies that Equation (17) is valid only over a corresponding range of ΔP_{ov}, and that when $\Delta P_{ov} \leq (4\sigma/D_{pws})(1 - K_2)$ the wicking potential will not decrease. Equation (17) can therefore be integrated to give:

$$\phi_{ws} = \overline{\phi}_{ws} \left\{ 1 - \frac{1}{K_2} \left[\frac{\Delta P_{ov}}{(4\sigma/D_{pws})} - (1 - K_2) \right] \right\} \qquad (32a)$$

for $\Delta P_{ov} \geq (1 - K_2)4\sigma/D_{pws}$, and

$$\phi_{ws} = \overline{\phi}_{ws} \qquad (32b)$$

It is evident from this discussion that more screen-related parameters are needed to characterize the wicking and breakdown behavior of a window screen than just D_{pws} and $C_{ws}/\overline{\phi}_{ws}$, the parameters usually measured and for which data are available. All the new parameters introduced here can be experimentally measured, however, and the test results given later show that the proposed relations agree with observed data. (In Ref. 2, a term F_σ was introduced that is equivalent to $\overline{\phi}/4$ and a term K_u introduced that is analogous to, but not identical with, K_2, and is dependent upon the start basket design).

2.5   Evaporation Rates

In space applications, the evaporation rate from the external surfaces of the main and window screens will be driven by heat transfer:

$$\dot{m}_0 = \dot{q}/h_{fg} \tag{33}$$

where $\dot{q}$ is the imposed heat rate per unit area, and h_{fg} is the heat of vaporization of the propellant. Depending on the test arrangement, $\dot{m}_0$ can also be driven by a heat flux in ground-based experiments; in general, however, $\dot{m}_0$ may not be directly related to a heat transfer rate and should therefore be measured independently.

The internal evaporation rate, $\dot{m}_e$, will not be created by a heat flux even in space, since the external main channels will "intercept" all the heat. For near-boiling liquids, the evaporation rate is instead a function of the difference between the saturation pressure of the liquid and the partial pressure of the vapor in the gas above the liquid (Ref. 11). Thus, it is proposed here to compute the internal evaporation rate by

$$\dot{m}_e = \alpha(P_{sat} - P)/\sqrt{RT} \tag{34}$$

where, typically, the empirical constant α ranges from about 10^{-4} to 1. For a liquid whose temperature is well below the boiling point, internal evaporation is probably negligible.

Since internal evaporation requires an energy transfer rate of $\dot{m}_e h_{fg}$ from the main liquid, the temperature of the main liquid must decrease. This complicated heat transfer problem within the main liquid depends on whether the start basket is in a low-gravity environment or not, and in any case is outside the scope of the present work. Instead, the liquid mass is idealized as a "well-stirred reactor", so that the temperature response is given by

$$\frac{dT}{dt} = -\dot{m}_e h_{fg} A_{vs}/\rho_L c_p V_L \tag{35}$$

(Equation (35) should best be used to correlate data or to study trends, because in fact the liquid will stratify with the colder liquid near the surface. Stratification is an important effect when making quantitative studies since the variation of P_{sat} for small changes in the temperature is easily of the same order of magnitude as the bubble-point of many window screens.) For parametric studies, P_{sat} can be computed from Antoine's equation (Ref. 12):

$$P_{sat} = E_1 \exp\left[-E_2/(E_3 + T)\right] \tag{36}$$

where the parameters E_1, E_2, and E_3 have been tabulated for most liquids (Ref. 13).

2.6   Flow Through the Window Screen

When either the pressure differential across the window screen exceeds the bubble-point or the central area of the window screen dries out, vapor will flow from the exterior into the basket. If the screen dries out, the inflow can be computed by a relation of the form of Equation (4) with the gas viscosity used rather than the liquid.

$$\dot{M}_V = 2\rho_L \Delta P_{ov} \, (L - \ell) \, B/\mu_o a_{ws} F_{ws} \tag{37}$$

This equation would be needed whenever the solution of Equation (26) yields $\ell < L$.

When the bubble-point is exceeded, a "dry" area cannot be identified, and the normal screen-flow equations of the type of Equation (37) are not valid. In Ref. (2), it has been proposed that the flow should be based upon the difference between ΔP_{ov} and the bubble-point pressure; thus

$$\dot{M}_V = 2\rho_L [\Delta P_{ov} - (\Delta P_{ov})_{max}] L B/\mu_o a_{ws} F_{ws} \tag{38}$$

Equation (38) appears to be reasonable, and does predict an increasing flow rate as ΔP_{ov} increases. It has one major deficiency, however, and

should be changed in several ways. The deficiency is that inflow will continue as long as ΔP_{ov} remains larger than the resealing pressure differential, $K_3(\Delta P_{ov})_{max} \approx 0.57 \ (\Delta P_{ov})_{max}$; Equation (38) predicts instead that the inflow ceases as soon as $\Delta P_{ov} \leq (\Delta P_{ov})_{max}$. That can be corrected by assuming that the inflow is proportional to $\Delta P_{ov} - K_4(\Delta P_{ov})_{max}$, where K_4, a new parameter defined here, cannot be greater than K_3. Sample calculations show that the predicted inflows are now substantially larger than those observed in tests. However, visual observations during bubble-point and start-basket testing have shown that the flow penetrates only a small fraction of the screen area; thus, the screen area 2LB in Equation (38) should be reduced by an area-fraction factor A_f. It is also probable that the resistance F_{ws} as computed for gas flow across a dry screen is much too small, since the screen is still visually wet. The correction factor K_f needed to account for this must be determined experimentally. The corrected method of computing the inflow is proposed to be

$$\dot{M}_v = 2\rho_L [\Delta P_{ov} - K_4 \ (\Delta P_{ov})_{max}] \ A_f LB/\mu_o a_{ws} F_{ws} \tag{39}$$

Equation (39) will be needed whenever ΔP_{ov} exceeds the bubble-point pressure before any part of the screen dries out.

2.7   Solution of Equations

The preceding set of algebraic and differential equations has been programmed for numerical solution, using a Runge-Kutta integration routine. Many sample problems were investigated. Some of the important findings include:

1.   When the window screen breaks down because P_{ov} at some instant exceeds the bubble-point pressure, the screen almost always is subsequently predicted to de-wick because ΔP_{oms} becomes larger than the wicking suction, $\phi_{ws}\sigma/D_{pws}$. (Equation (10) shows that $\Delta P_{oms} \geq P_{ov} - \Delta P_{\ell v} + \rho_L gh$ and the wicking suction pressure of any screen is less than its bubble-point pressure.) The pressure differential ΔP_{ov} across the screen then rapidly changes to a new value such that $\phi_{ws}\sigma/D_{pws} - \Delta P_{oms} = 0$, and then the de-wicking is halted. The percentage of dry area adjusts itself

so that the inflow rate is just sufficient to maintain ΔP_{ov} with this new area. Note that the net wicking suction is zero, so the screen will not re-seal. It is unlikely that the model exactly predicts the real behavior of the window screen, since the channel suction ΔP_{oms} cannot rupture the liquid layer in the window screen. Instead, the thickness of the layer would just decrease as liquid is pulled into the channels, and the screen would remain sealed for an extended period. The thinning of the liquid layer would, however, decrease the bubble-point pressure, and the response of the window screen might therefore be erratic.

In order to study the other parameters, the dewicking effects of ΔP_{oms} were suppressed in the calculations described in the following cases.

2.   The response of the window screen is very sensitive to the rate of internal evaporation, and it is possible to select the proportionality constant, α, in Equation (34) such that inflow is completely prevented. This can be seen by combining Equations (1), (3), and (34) to give:

$$V \frac{dP}{dt} = \alpha A_{vs} \sqrt{RT} (P_{sat} - P) - PA_i \frac{dh}{dt} + RT\dot{M}_v$$

Initially, there is a rapid decrease in the vapor space pressure from P_{sat} to $P_{sat} - \Delta P_{ov}$. The magnitude of ΔP_{ov} can be controlled at any desired fraction of $(\Delta P_{ov})_{max}$; inflow will be prevented ($\dot{M}_v = 0$) by choosing α in accordance with

$$\alpha \geq P_{sat} A_i (dh/dt)/A_{vs}\sqrt{RT} \Delta P_{ov}$$

Since $\sqrt{RT}$ is a large number, the computed values of α are within the reasonable range of 10^{-4} to 1.0.

3.   Cycling of the inflow (that is, alternating periods of window screen breakdown and re-sealing) cannot occur when the window screen dries out from evaporation (Equation (25)). Instead ΔP_{ov} and the dry area approach constant values such that the inflow maintains a balance with the rate of increase of the vapor space volume.

4.   If $K_4 = K_3$, cycling of the inflow cannot occur even when the breakdown is caused by $\Delta P_{ov} \geq (\Delta P_{ov})_{max}$ (Equation (30)). Instead, P_{ov} approaches a constant value just larger than $K_3 (\Delta P_{ov})_{max}$ so that the volume of gas admitted is again equal to the volume of vapor space made available, as in Case 2 above.

5.   If $K_4 < K_3$, cycling of the inflow is possible. The pressure difference $\Delta P_{ov} - K_4 (\Delta P_{ov})_{max}$ always remains greater than zero, with the result that after an initial sharp drop of the vapor space pressure, the inflow rate is larger than that needed to balance dV/dt and the vapor space pressure begins to increase. At some point, ΔP_{ov} increases to $K_3 (\Delta P_{ov})_{max}$, and the screen re-seals. The process then repeats itself.

Figure 2 shows some results for a typical case 5. As can be seen, short periods of inflow are followed by much longer periods when the window screen remains sealed. (Internal evaporation has been set equal to zero in these computations in order to emphasize the cyclical response.) The time duration of the inflow periods (in seconds) is 0.0082V, where V is in cm^3, while the duration of the sealed window periods is 4.4V. The cycling frequency is short initially but increases as the vapor space volume increases. For these computations, K_4 has been taken as 0.56, K_3 as 0.57, A_f as 10^{-2}, and K_f as 10^3. The periods of inflow are proportional to K_f/A_f, so if either K_f is decreased or A_f increased, the inflow time can be decreased substantially.

Cases 1, 3, 4, and 5 apply to either cryogenic or storable liquids. For a cryogenic liquid, there is also a very slow decrease in the vapor space pressure superimposed on the other pressure changes resulting from the decrease of P_{sat} as the main liquid cools to supply the energy needed to support the internal evaporation.
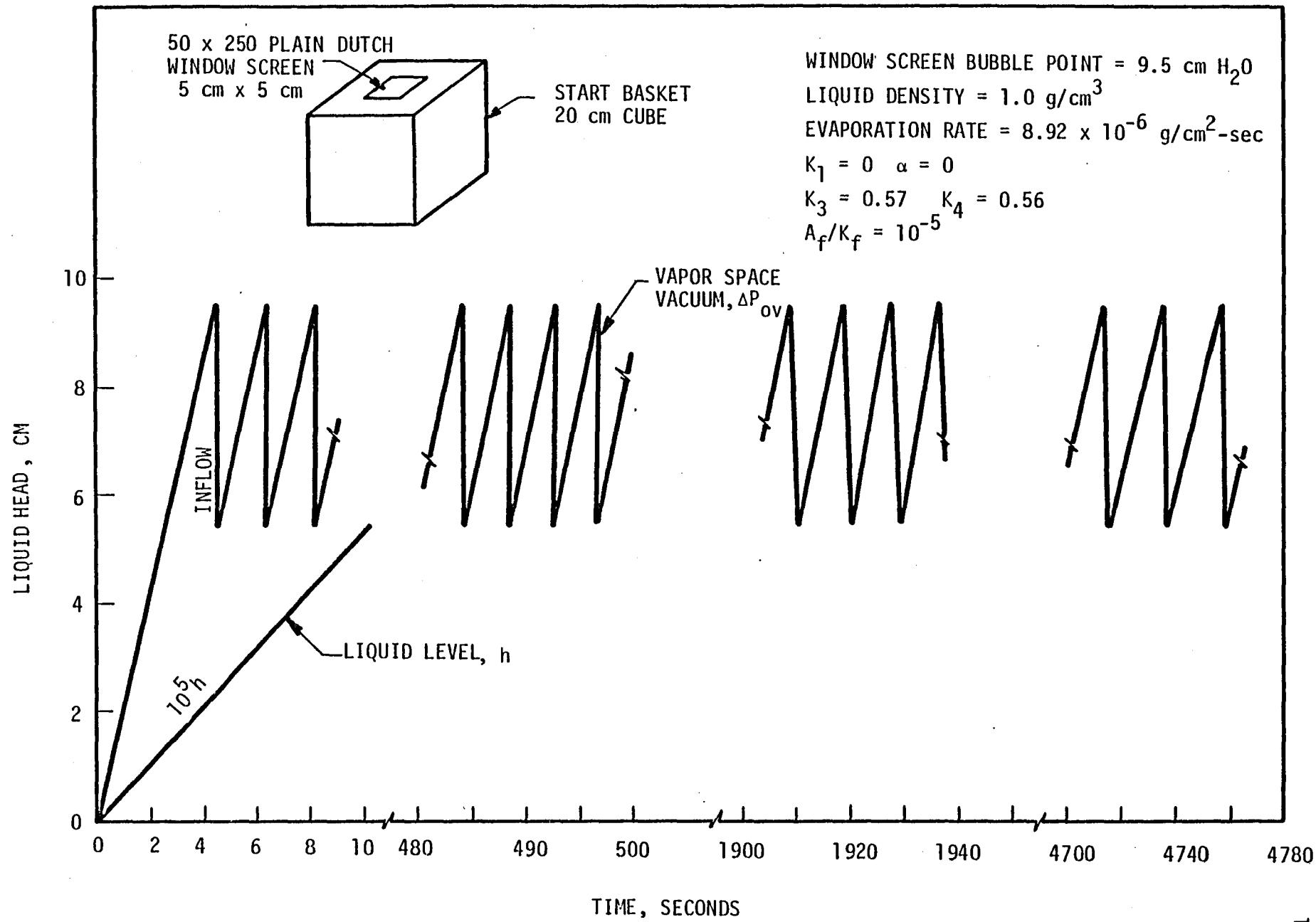
FIGURE 2. TYPICAL CYCLICAL INFLOW

3. EXPERIMENTAL PROGRAM, RESULTS, AND DISCUSSION

The experimental program had two main objectives:

1. Validate the various original analytical sub-models and determine the empirical constants contained in them, and
2. Verify the predictions of the entire analytical model for a simulated start basket.

The first objective was met by a series of separate-effects tests using several different experimental apparatus. A simplified start basket was built and tested to meet the second objective.

Two window screen candidates were used in these tests separately and in conjunction with two main screen candidates:

-   50 x 250 plain dutch (window)
    165 x 800 twilled dutch (main)
-   24 x 110 plain dutch (window)
    200 x 1400 twilled dutch (main)

The 24 x 110/200 x 1400 combination has a much greater difference in screen bubble points than does the 50 x 250/165 x 800 combination. Two different liquids, one volatile and one non-volatile, were used in the tests in order to study the effects of evaporation:

-   isopentane (boiling point = 28°C)
-   ethanol (boiling point = 118°C)

The relevant properties of these liquids are listed in Table 1.

The test screens were washed, cleansed, and dried using the procedures described in Ref. 8. All tests were conducted in a small laboratory having controlled temperature and humidity conditions.

Table 1. Properties of Test Liquids at 20°C

Liquid	Density g/cm^3	Viscosity dyne-sec/cm^2	Surface Tension dyne/cm
Ethanol	0.789	0.012	22.3
Isopentane	0.625	0.0022	16.1

3.1 Separate-Effects Tests

In the separate-effects tests, experimental determinations were made of:

1. Wicking resistance coefficient, C
2. Wicking pressure constant, $\bar{\phi}$
3. Bubble-point diameter, D_p
4. Effective flow thickness, b_f
5. Decrease of bubble-point pressure due to wicking, K_2
6. Decrease of wicking pressure due to pressure differential, K_1
7. Flow resistance of window-screen/main-screen joint, F_j
8. Degradation, if any, of window-screen bubble-point due to the joining method

Items 4, 5, and 6 were measured only for the window-screen candidates since they are not needed in the analysis of the main screens.

Data on some of the required coefficients are available in the literature for some screen types (for example, $C/\bar{\phi}$ and D_p). Those data served as validation checks on the test methods of this study.

Wicking Characteristics. The wicking resistance C and the wicking pressure constant $\bar{\phi}$ were measured with the "Screen and Joint Characterization" apparatus shown in Figures 3 and 4. During tests, the apparatus was enclosed in a large, clear plastic box containing several sponges soaked in the test liquid. The tests were not started until the liquid vapors had saturated the

air in the box. (The hypodermic syringe shown in the figure was outside the box.)

In the horizontal configuration, a test screen was clamped over a small reservoir in the apparatus, stretched over a knife edge, and held horizontal by a set of clamps attached at the other end to a long, threaded rod. The reservoir was filled initially until the liquid surface almost touched the screen. To start a test, additional liquid was rapidly added to the reservoir, using the hypodermic-like syringe shown in Figure 3, until the liquid surface was level with the knife edge; liquid would then wick along the length of the screen. The reservoir level was maintained at the knife edge during the entire test. The leading edge movement of the wicking liquid as a function of time was measured with a stop watch and a 0.1 inch (0.25 cm) graduated scale (not shown) attached to the clamps immediately above the screen. The test was continued until the wicking velocity became very small or until it was apparent that evaporation had started to become important.

In the vertical configuration, the test procedures were similar except the knife edge was not needed. It was found that liquid would not wick past the top edge of the clamp that formed one wall of the reservoir. ' Thus, the reservoir was filled to a level just below the top of the clamp; the test was started by subsequently adding just enough liquid to bring the level even with the top of the clamp. Liquid would then wick up the vertical screen. The wicking suction pressure was eventually balanced by the gravity head of the wicked liquid, so the wicking came to a definite stop.

Figures 5 and 6 show typical results of the horizontal wicking tests. Measured wicking distances are plotted against the square root of wicking time, since, as shown by Equation (14), such plots should result in straight lines. The slopes of the straight lines are related to the wicking parameters by:

$$\frac{C}{\phi} = \frac{2\sigma b^2}{\mu_L D_p} (SLOPE)^{-2} \tag{40}$$
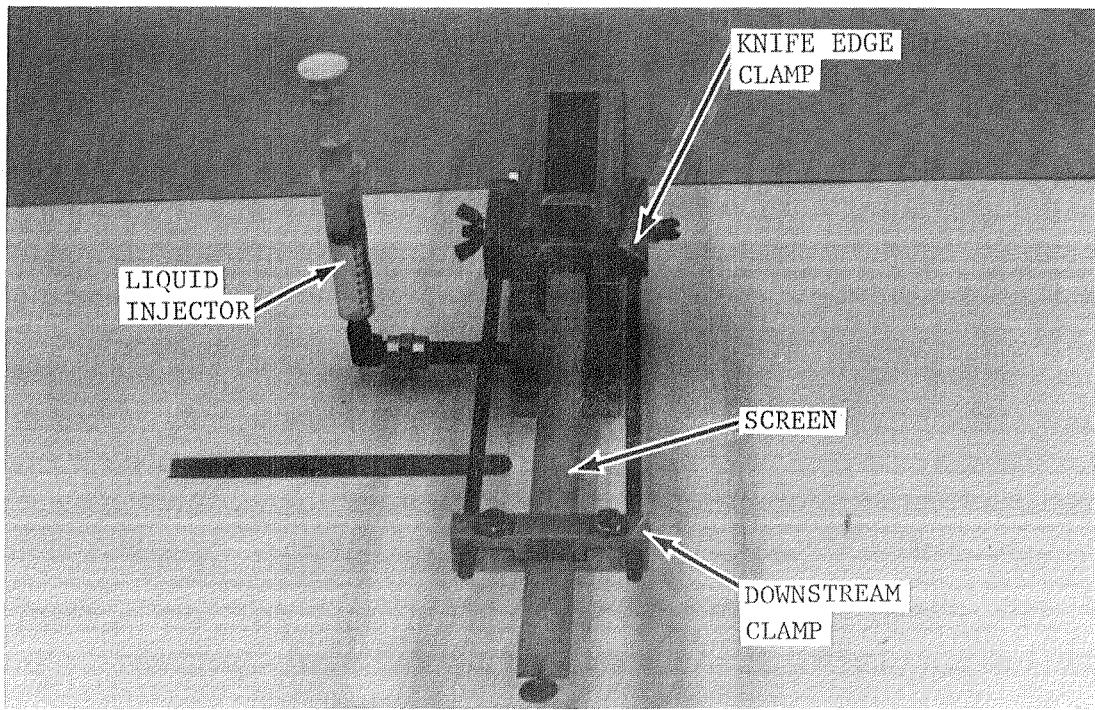
a. Overall View
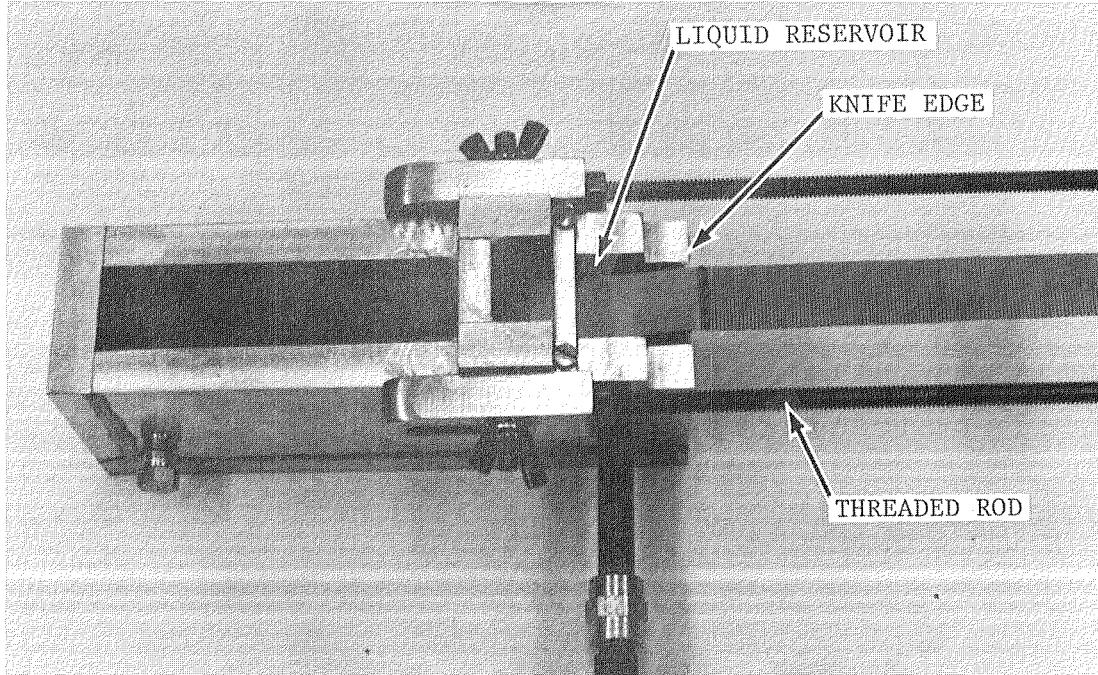
b. Close-up of Knife-Edge End

FIGURE 3. HORIZONTAL CONFIGURATION OF "SCREEN AND
JOINT CHARACTERIZATION" APPARATUS
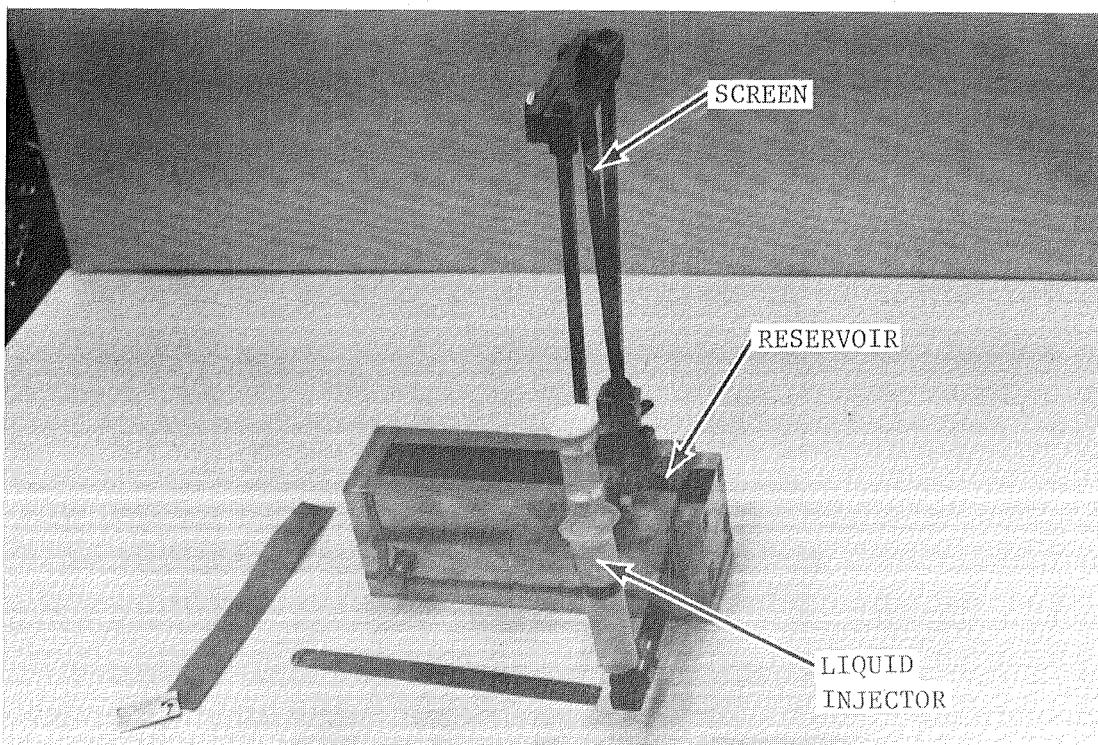
a. Vertical Configuration
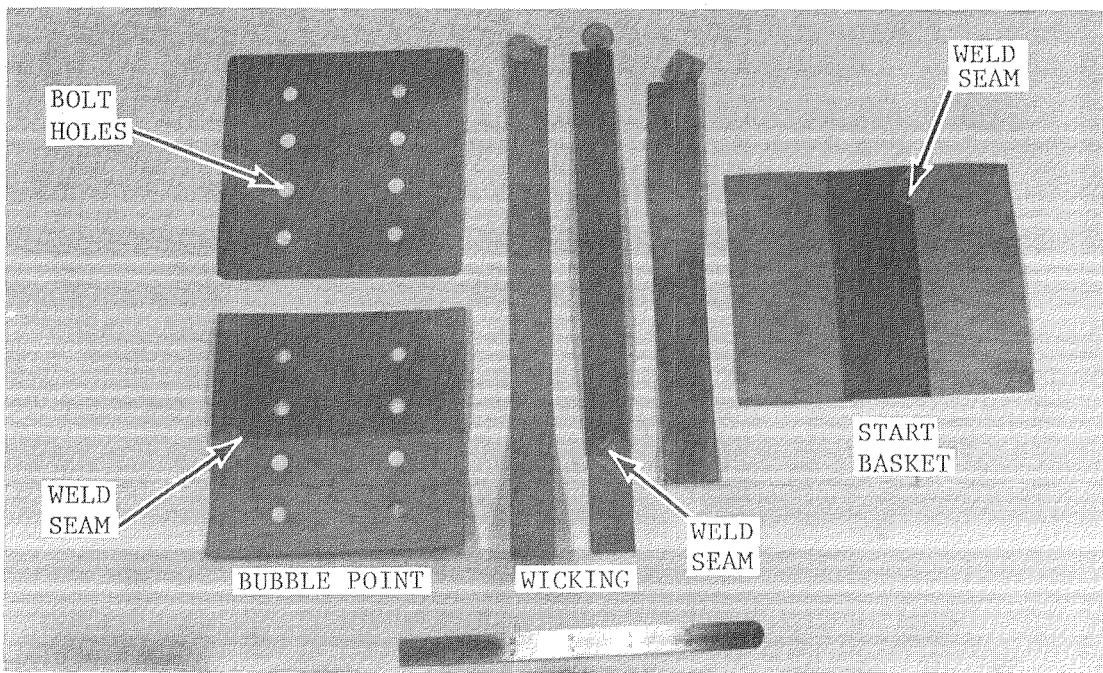
b. Screen Samples

FIGURE 4. VERTICAL CONFIGURATION OF "SCREEN AND JOINT
CHARACTERIZATION" APPARATUS AND SCREEN SAMPLES
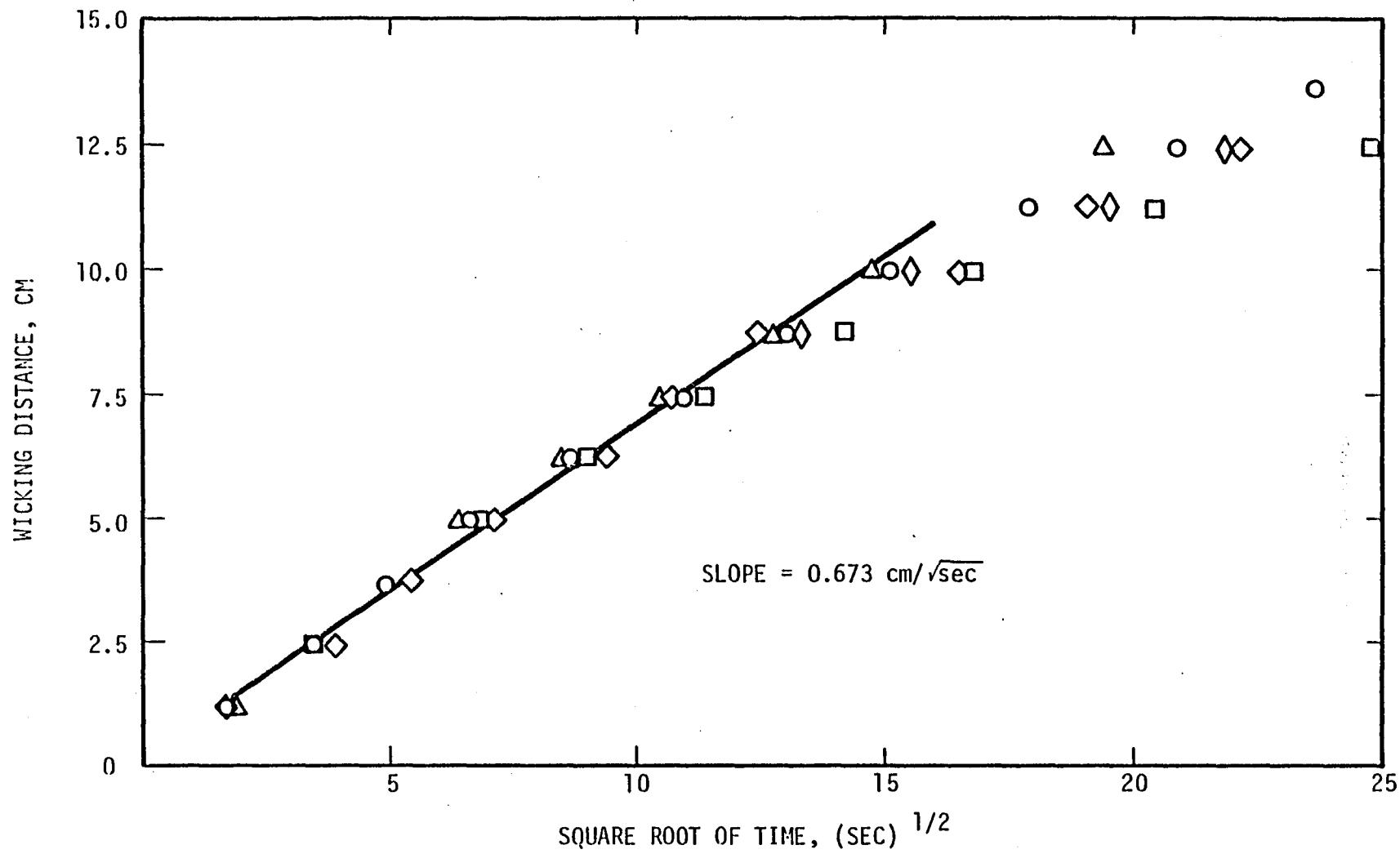
FIGURE 5. ETHANOL WICKING PERPENDICULAR TO WARP WIRES OF 165 x 800 DUTCH TWILL SCREEN
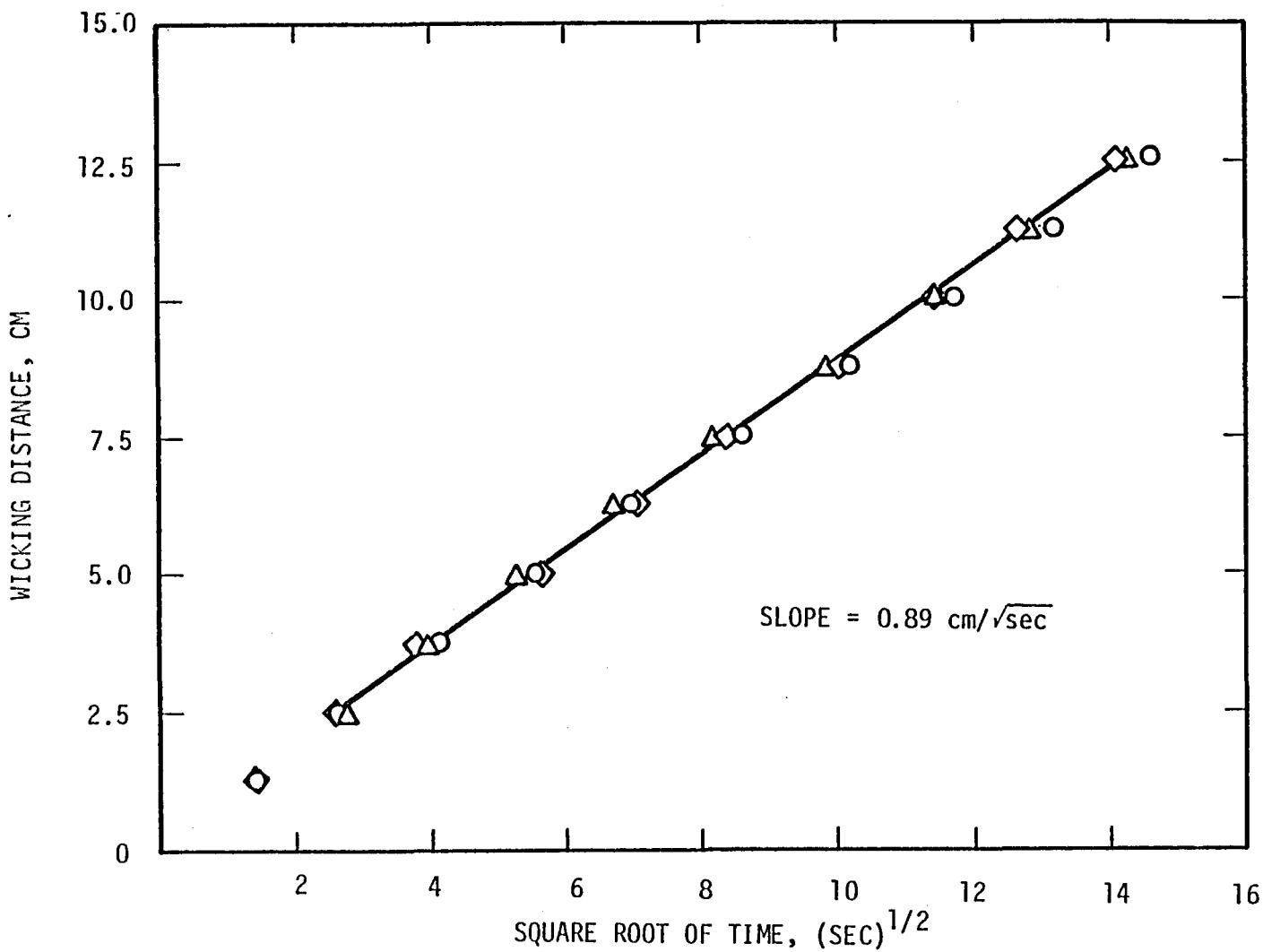
FIGURE 6.   ETHANOL WICKING PERPENDICULAR TO WARP WIRES OF 24 x 110 PLAIN DUTCH SCREEN

By measuring the bubble-point diameter separately, the plots can therefore be used to compute $C/\bar{\phi}$.

The repeatability of these data from test to test was good, with the exception that some difficulty was experienced occasionally in starting the wicking in a repeatable way; near the end of the tests, evaporation of the liquid also caused some data scatter. On the whole, tests of ethanol gave less scatter than isopentane because of the rapid evaporation of isopentane; even so, the computed slopes for both liquids for a given screen were in reasonable agreement with the σ/μ_L ratios. Only the ethanol test results were used to compute $C/\bar{\phi}$. The parameter group $(\bar{\phi}/C)b^2/D_p$ has been measured in a previous study for all the screen weaves used here (Ref. 8); that study gave results either equal to the results computed from the present test or up to about forty percent larger, but never smaller. Differences in the way the test data were analyzed may account for the discrepancies, since in Ref. 8 the wicking velocity, a quantity derived from the test measurements, was plotted against the wicking distance to determine $(\bar{\phi}/C)b^2/D_p$, in accordance with Equation (12).

The parameter $\bar{\phi}$ can be determined by measuring the maximum wicking distance, H_{max}, obtained during vertical tests (Figure 4). At that point, the hydrostatic head just balances the wicking suction pressure. Thus:

$$\bar{\phi} = \rho_L g H_{max} D_p / \sigma \qquad (41)$$

Measured values of H_{max}, again from the ethanol tests, are shown in Table 2. Each measurement is the average of at least three tests using different screen samples. Isopentane did not give reliable results because the wicking velocity was so slow in comparison to the evaporation rate that the liquid turned to ice on the screen as a result of evaporative cooling. It might be noted that the wicking height, and therefore $\bar{\phi}$, for all but the 200 x 1400 screen was larger for wicking perpendicular to the warp wire than for wicking parallel to it.

Values of the parameters C and $\bar{\phi}$, computed from the test data by using Equations (40) and (41) in conjunction with the bubble-point diameter

Table 2. Maximum Vertical Wicking Distance For Ethanol
Wicking Perpendicular or Parallel to Warp Wire

	Screens							
	24 x 110		50 x 250		165 x 800		200 x 1400	
	Perp.	Par.	Perp.	Par.	Perp.	Par.	Perp.	Par.
H_{max}(cm)	0.56	0.46	1.08	0.64	8.13	6.86	3.43	4.83

measured in tests discussed later, are given in Table 3. Note that the
wicking suction-pressure constant $\bar{\phi}$ varies from less than one-tenth
to about one-fourth of the bubble-point pressure constant (i.e., 4),
depending on the screen weave and wicking direction. The wicking resistance
of the screen, C, tends to increase for the more closely woven screens, as
might be expected.

Joint Flow Resistance

To determine the concentrated flow resistance of typical window-
screen/main-screen junctions, samples of the 50 x 250 and 165 x 800 screens
were joined by electrical-resistance spot welding, as were the 24 x 110 and
200 x 1400 screens. All possible combinations of warp and shute wire
intersections were evaluated; likewise, the spacing of the weld spots was
varied from about 0.6 cm to 0.3 cm. Figure 4b shows a representative sample
of welded screens used for these tests and others as described later.
(Figures 3a and 3b show, in fact, a test using a 24 x 110 screen joined to
a 200 x 1400 screen rather than a single screen.) Tests were conducted
only in the horizontal configuration.

The test screens were inserted in the apparatus so that the screen
junction was within 0.16 cm or so of the downstream side of the knife-edge,
in order to minimize the effects of the wicking resistance of the upstream
screen. It was not possible to bring the junction closer than about 0.16 cm,
however, because the meniscus formed by the liquid at the intersection of
the knife-edge and the screen would otherwise extend downstream of the junc-
tion and invalidate the tests. The effective resistance of the 0.16 cm
length of upstream screen on the wicking in the downstream screen can be
evaluated by making a wicking pressure and flow balance, using methods

Table 3. Wicking Flow Characteristics

Screen	Thickness, b	Bubble Point Diameter, D_p	Wicking Direction Relative to Warp Wire	C	$\overline{\phi}$	$b(12/C)^{1/2}$	b_f
50 x 250	368×10^{-4} cm	105×10^{-4} cm	Perpendicular	338	0.393	69×10^{-4} cm	143×10^{-4} cm
			Parallel	584	0.231	52×10^{-4} cm	Not Determined
24 x 110	940×10^{-4} cm	275×10^{-4} cm	Perpendicular	507	0.428	144×10^{-4} cm	118×10^{-4} cm
			Parallel	1369	0.533	88×10^{-4} cm	Not Determined
165 x 800	147×10^{-4} cm	40×10^{-4} cm	Perpendicular	476	1.128	23×10^{-4} cm	"
			Parallel	1548	1.047	13×10^{-4} cm	"
200 x 1,400	135×10^{-4} cm	19×10^{-4} cm	Perpendicular	1962	0.225	10.6×10^{-4} cm	"
			Parallel	1525	0.318	12.0×10^{-4} cm	"

similar to those described previously. The result is that the wicking distance is now not directly proportional to the square root of time, but is instead:

$$L_1 = \left\{ 2 \left(\frac{\sigma t}{\mu}\right)\left(\frac{\phi b}{CD_p}\right)_1 + \left[\frac{F_j b_1^2}{C_1} + \left(\frac{C_2}{C_1}\right)\left(\frac{b_1}{b_2}\right)^2 L_2\right]^2 \right\}^{1/2}$$
$$- \left[\frac{F_j b_1^2}{C_1} + \left(\frac{C_2}{C_1}\right)\left(\frac{b_1}{b_2}\right)^2 L_2\right] \tag{42}$$

where the subscript 1 indicates the downstream screen and the subscript 2 the upstream screen. When the 50 x 250 screen or the 24 x 110 screen is upstream, the effect of $L_2 \approx 0.16$ cm is negligible. But when the 165 x 800 or 200 x 1400 screen is upstream, the factor multiplying L_2 can be very large; for example, when the wicking is parallel to the warp wires of both screens, a length of 200 x 1400 screen of 0.16 cm represents an equivalent length of 8.6 cm of 24 x 110 screen upstream of the weld line. When analyzing test data, these effects must be included, or else the resistance of the upstream screen would be assinged to the joint.

Figure 7 shows typical results for wicking from a window screen to a main screen across the welded joint. As can be seen, the wicking data virtually overlays the straight lines determined from the tests of the window screen alone. The concentrated resistance of the joint is negligible. Figure 8 shows, on the other hand, results of wicking from a main screen to a window screen. The effects of the large effective resistance of the small length of the upstream main screen are evident in these tests; while neither the concentrated resistance of the joint nor the actual length of 200 x 1400 screen can be determined from these tests, the results are consistent with $F_j \approx 0$ for realistic values of L_2. Since all the tests of wicking from a window screen to a main screen indicated that $F_j \approx 0$, it is concluded that the joint resistance is negligible.

Bubble-Point

Although available for some of the screens of interest (Refs. 4, 14), the bubble-points for all the screens were measured in this study in order
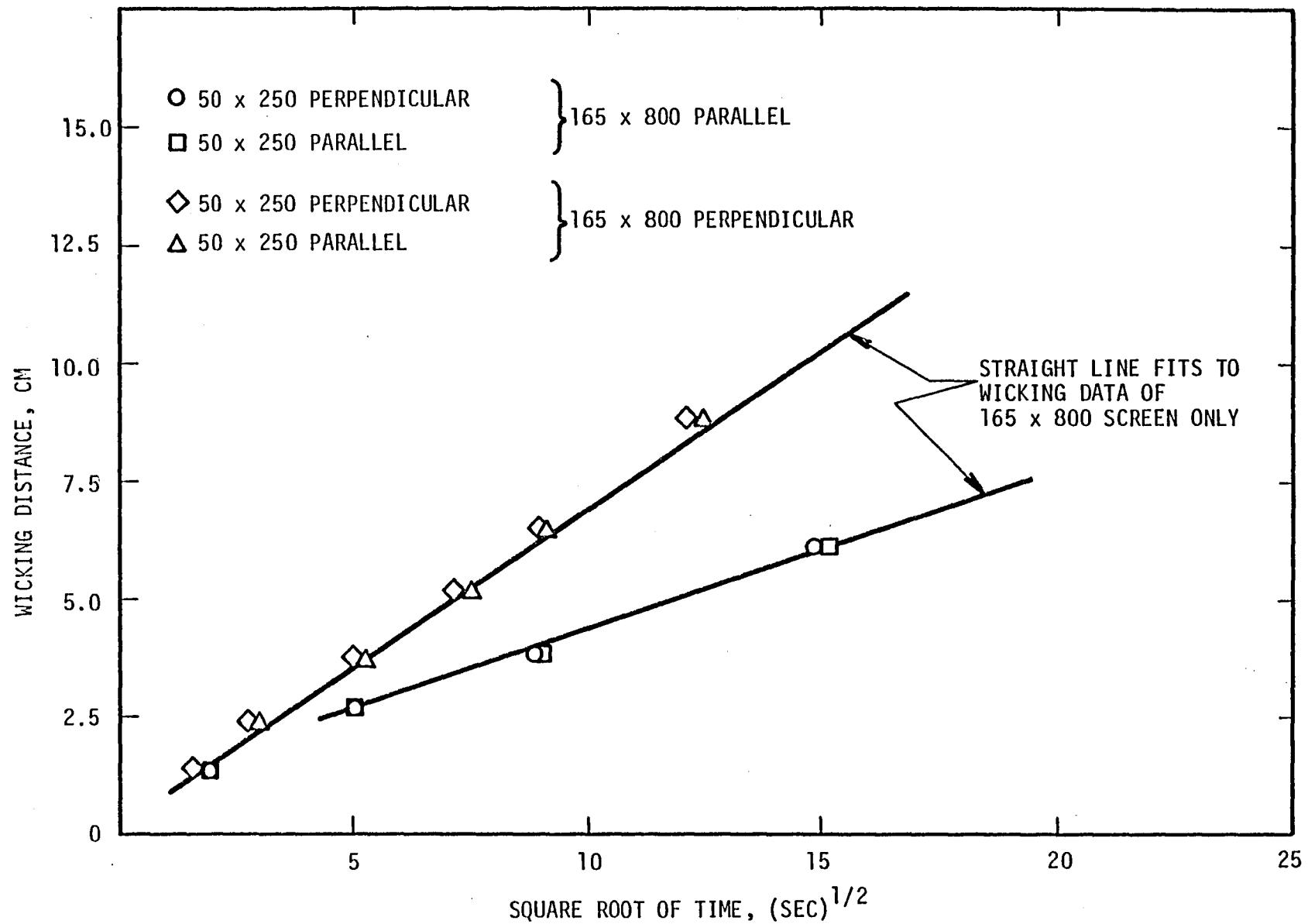
FIGURE 7. ETHANOL WICKING FROM 50 x 250 SCREEN TO 165 x 800 SCREEN
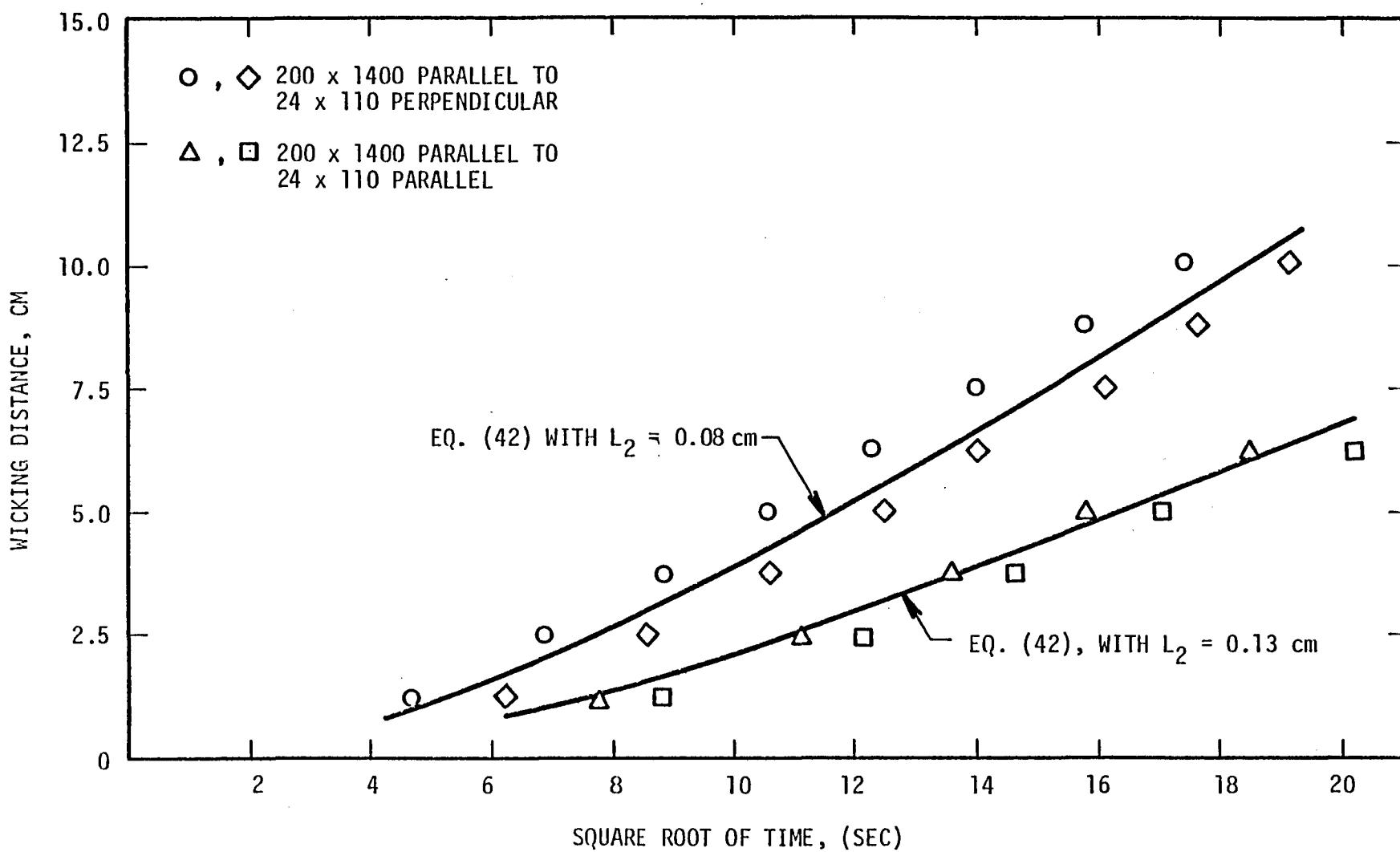
FIGURE 8. ETHANOL WICKING FROM 200 x 1400 SCREEN TO 24 x 110 SCREEN

to have a common basis for determining the change in bubble point caused
by evaporation. Figure 9 shows the apparatus used for these tests.

To determine the bubble-point, a sample screen was inserted into the
apparatus between rubber gaskets and bolted down, using vacuum grease on
the gaskets when required to make a leak-proof seal. Ethanol or isopentane
was then poured on the screen to form a pool 0.6 cm deep. The pressure in
the plenum chamber below the screen was increased slowly, by manually
depressing the plunger of the large hypodermic-like syringe. Chamber
pressure was measured by a water manometer. The pressure at which gas bubbles
visually penetrated the liquid was taken as the bubble-point, after
correcting for the 0.6 cm head of liquid on the screen. Each bubble-point
was determined using three different samples of screen for each test liquid.
There was little or no scatter in the data, and the ethanol and isopentane
results were consistent. It was noted that the chamber pressure had to be
reduced in order to make the screens re-seal, in agreement with the obser-
vations given in Ref. 10.

The computed bubble-point diameters are shown in Table 3. They are
the same or slightly smaller (that is, the bubble-point pressures themselves
were larger) than the test results given in Ref. 4, thereby implying that
the testing technique was adequate and the apparatus free of leaks.

Combinations of window and main screens were also tested, with the
joints fabricated as described previously. For the 24 x 110/200 x 1400
screen combination, there was no measurable reduction in the bubble-point
in comparison to the 24 x 110 screen alone. For the 50 x 250/165 x 800
combination, a 17.5% reduction was found when the spacing of the weld spots
was 0.63 cm, but there was no measurable reduction for spacings of 0.3 cm
or less. Even though the bubble-point of the combinations could be made
equal to the window screen alone, visual observations showed that the bubbles
always broke through the welded seam first. The seam therefore apparently
always represents the largest "pores".

Next, a series of tests were conducted to determine the parameter K_2,
(Equations (26), (27), or (29)) that represents the decrease of bubble-point

34
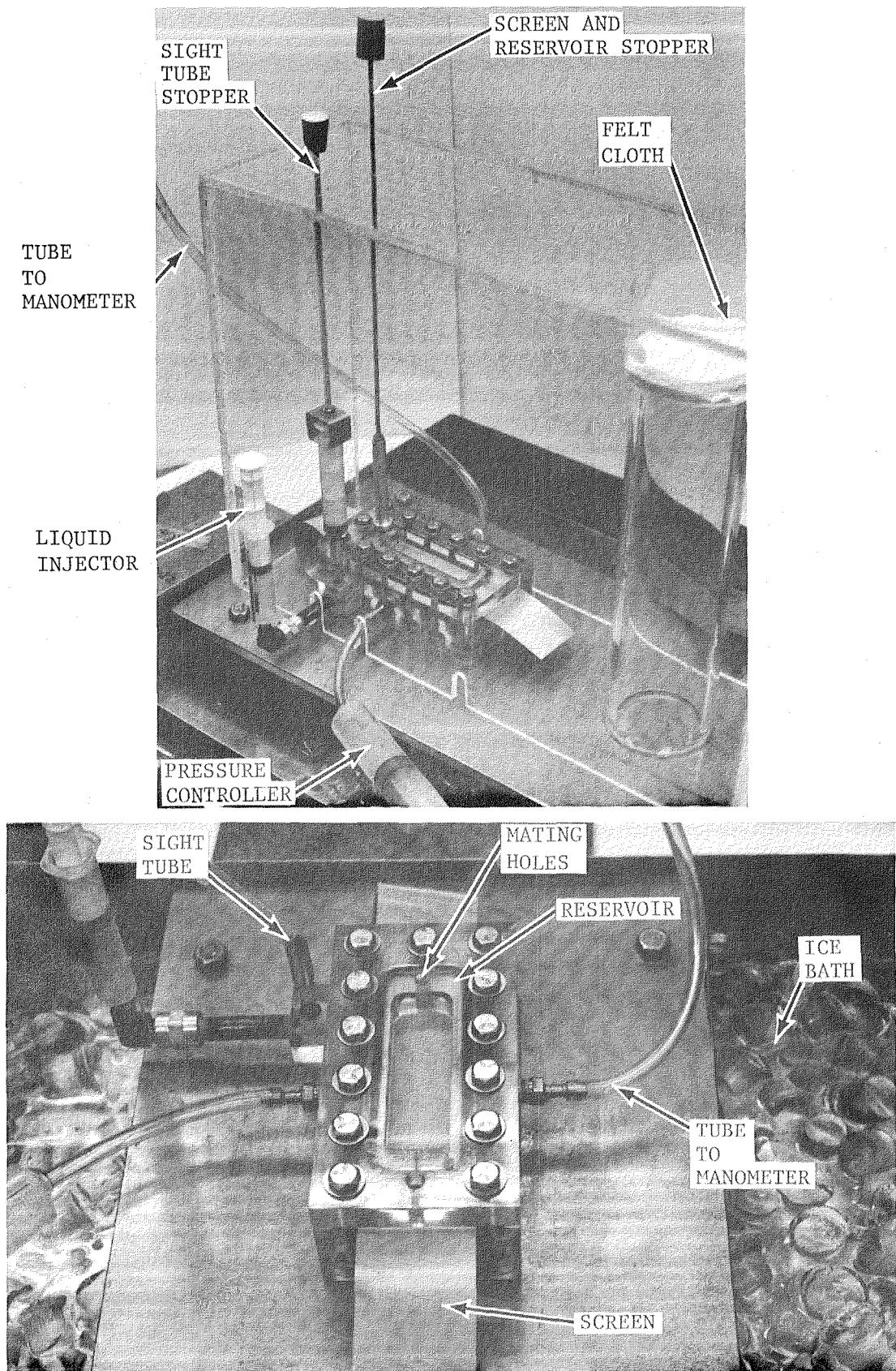
FIGURE 9. "BUBBLE-POINT/WICKING/EVAPORATION" APPARATUS

pressure when the screen is wicking. To measure K_2, several different evaporation rates had to be established in fully wet screens, in order to vary the wicking velocity. It was quickly found that the method originally proposed for creating a specified evaporation rate, electrical-resistance heating, was not feasible. The available DC current generator could not pass a current through either window screen that was large enough to raise its temperature to the boiling point of ethanol. On the other hand, with isopentane the difficulty was not in heating the screen but in correlating the resultant evaporation rate with the electrical heating rate, since isopentane boils without heating at just above room temperature. The test plan was therefore modified. The tests using ethanol were abandoned, and the evaporation rate of isopentane was regulated by placing the entire apparatus in an ice bath. By removing the ice and letting the apparatus slowly heat to room temperature, a series of tests with increasing rates of evaporation could be conducted.

The small reservoir noted in Figure 9 was used to supply wicking liquid to the screen for these tests. A knife-edge, over which the screen was clamped, was used to separate the reservoir from the plenum chamber. Each screen contained a 0.32 cm drilled hole in the end clamped over the reservoir, which was aligned with a similar hole in the plastic cover over the reservoir; see Figure 9. The purpose of these holes was to relieve the pressure in the reservoir as liquid boiled off during the relatively long time needed to determine the evaporation rate from the screen.

The sequence of events used to conduct a test is explained with the aid of Figure 9.

1.   The entire air volume within the plastic enclosure was saturated with isopentane vapor by soaking with isopentane a felt cloth in the dish that can be seen atop the tall plastic cylinder. Isopentane vapor, which is heavier than air, slowly forced out most of the air through several small ports at the bottom of the enclosure.

2.   The liquid reservoir was filled by injecting liquid from a hypodermic-like syringe operated from outside the enclosure. The mating holes in the screen and the reservoir cover were then sealed by a plunger, also operated from outside the enclosure. The plunger was composed of (1) a small-diameter rubber-tipped cylinder that pressed down on the screen and connected by an internal spring to (2) a larger rubber-tipped cylinder that pressed down on the reservoir cover. Lowering the long rod outside the enclosure that was attached to these cylinders thus sealed the screen and the reservoir. The glass sight-tube connected to the liquid reservoir was similarly sealed by a rubber-tipped cylinder attached to a syringe-like device that was also operated externally, as indicated in Figure 9.

3.   Additional liquid was added to the reservoir from the syringe and forced over the knife edge until a standing pool 0.64 cm deep was formed above the screen. A bubble-point test was then conducted in the normal way.

4.   The standing pool of isopentane was allowed to evaporate, after which the mating holes in the screen and the reservoir were unsealed, as was the sight tube. The liquid reservoir was refilled as necessary, being careful to keep the liquid level at the knife-edge by observing the sight-tube.

5.   While maintaining the liquid level in the reservoir at the knife-edge in order to form a supply of liquid for wicking, the isopentane on the screen was allowed to evaporate until one cc of liquid had been injected into the reservoir from the graduated syringe. The total time needed to do this was noted.

6.   The sight tube and the mating holes in the screen and the reservoir were sealed as before. Immediately, the lower chamber was pressurized until gas penetrated the screen, as evidenced by the rapid drop in the manometer reading. (There were no visible bubbles in this case since the screen was not submerged.) The screen continued to wick during this bubble-point test since the duration was not long enough to let the reservoir level drop below the knife edge. This measurement concluded a test.

7.   The temperature of the apparatus was allowed to increase and the entire test sequence repeated. Testing was continued until the apparatus reached room temperature. Typically 30 to 40 minutes were required for the temperature to change 1°C, while each test required 5 to 6 minutes; the temperature and the evaporation rate therefore did not change appreciably during a test.

The test measurements are presented in Table 4. Evaporated volumes could be measured to within 0.05 cm^3, which corresponds to an uncertainty in $\dot{m}_e$ of about 3.1 x 10^{-6} g/sec-cm^2 for the larger evaporation rates and 1.5 x 10^{-6} g/sec-cm^3 for the smaller ones; the uncertainty in the evaporation, thus, is less than three percent. The entries labeled $(\dot{m}_e)_{max}$ are the observed rates for which it appeared that any further increase would not have allowed the screens to remain wicked over their entire lengths. Since the evaporation rate could not be adjusted arbitrarily, there is some judgment involved in the decision as to what was $(\dot{m}_e)_{max}$.

For both screens, the measured decreases in the bubble-point indicate that $\beta_2 = 0.5$ (and thus $\beta_1 = 2.0$), although the fit of the data to this correlation is better for the 50 x 250 screen. Note that the computation of β_1 is not critically dependent upon the chosen value of $(\dot{m}_e)_{max}$, since the variation of bubble-point and evaporation rate from test to test can also be used to determine β_1. Data for the two main screen candidates and for the window screens in their less effective direction were not acquired since β_1 and β_2 are not needed for them in applications.

The effective open thickness, b_f, of the window screens was computed from the $(\dot{m}_e)_{max}$ data by the use of Equation (25) with $\ell = L = 7.62$ cm, the length of test screen, since this length is the maximum possible wicking length; both F_j and ΔP_{oms} were set equal to zero to correspond to the test set-up. Equation (25) gives for these conditions:

$$b_f = \frac{D_p}{\phi \sigma} \left[\frac{u_L L^2 C (\dot{m}_e)_{max}}{2 \rho_L b^2} \right] \tag{43}$$

Table 4. Decrease of Maximum Pressure Differential as a
Function of Evaporation Rate; Wicking Perpendicular to Warp Wire

Screen	Evaporation Rate $g/sec-cm^2$	Bubble Point (cm of H_2O)	Maximum ΔP (cm of H_2O)
50 x 250	6.61×10^{-5}	6.1	6.1
	7.54×10^{-5}	6.1	5.33
	$3.37 \times 10^{-4} (\dot{m}_e)_{max}$	6.1	3.05
24 x 110	7.08×10^{-5}	2.5	2.5
	8.78×10^{-5}	2.5	2.50
	1.52×10^{-4}	2.5	2.30
	2.16×10^{-4}	2.5	2.03
	$4.65 \times 10^{-4} (\dot{m}_e)_{max}$	2.5	1.25

The values of b_f so determined are also shown in Table 3, as well as the values of $b(12/C)^{1/2}$ derived from a capillary channel analogy. As can be seen, the channel analogy yields b_f values that are not markedly different from the measured ones, and thus $b(12/C)^{1/2}$ could be used as an estimate of b_f in the absence of other data.

3.2 Start-Basket Tests

At the conclusion of the separate-effects tests, a simulated start basket was constructed and tested (1) to demonstrate the interaction between the wicking flow, the evaporation rates, the the window screen inflows, and (2) to verify the general predictions of the model. The simplified design consisted of a window screen attached to a set of main screens that remained in contact with liquid throughout a test. Evaporation from the exterior surfaces of an actual start basket was simulated by draining liquid at a controlled rate from the main liquid volume.

Figure 10 shows the simulated start basket and some of the test in-strumentation. Both the main liquid volume and the two channel volumes were 2.54 cm by 7.62 cm in cross-section and 45.7 cm deep. The channel and main liquid volumes communicated along their entire depth through a series of 1.27 cm diameter holes drilled in the walls separating the volumes, with a vertical spacing of 7.62 cm between holes; the first set of holes was located 3.81 cm below the screens. The effective depth of the start basket could be controlled by blocking all the holes above any specified height; most of the tests were conducted with an effective depth of 34.3 cm. This head, which exceeded the bubble-point pressure of all but the 200 x 1400 screen, was more than sufficient to allow gravity draining from the main channel through the central drain and fill line over a wide range of simulated evaporated rates.

The window and main screens were held in place over knife-edges by rubber gaskets that were compressed by a set of upper and lower plastic clamps; the clamps were bolted together with substantial force, and in addition the gaskets were wetted with vacuum grease to help form a leak-tight

seal. The upper clamp, moreover, was fitted with two small diameter wires that pressed the screens tightly against the knife-edges. Proof tests showed that the clamping arrangement and the knife edges were leak tight for vacuum pressures equal to at least the bubble-point of the 200 x 1400 main screen. Wicking from the main screens to the window screens did not appear to be affected by the clamping pressure at the knife edges. The screen end of the apparatus was covered by a plastic enclosure, containing felt cloths soaked in the test liquid, to provide a controlled environment.

The pressure in the main liquid volume was measured by a diaphragm type of electronic pressure transducer connected to a digital voltmeter. Pressure differences of about 0.3 cm of liquid could be measured readily. The level of liquid in the main volume was read directly from graduated scales attached to the exterior walls; the accuracy of these readings was about ±0.25 cm. The liquid drained from the main volume into a graduated cylinder (not shown) which provided an independent check of the liquid level readings. Test times were determined from a stop watch. For tests using isopentane, the entire apparatus was cooled for several hours in a freezer before conducting tests, in order to control the evaporation rate; otherwise boiling in the channel volumes rapidly made the tests invalid. At the start of a test, all three volumes were completely full of liquid and contained no visible bubbles.

A complete set of tests was conducted initially with the window screens spot-welded to the main screens, as shown in Figure 4b. The weld seams were located over the main liquid volume, very near and parallel to the knife-edges. These tests gave repeatable data, but visual observations showed in every case that exterior gas broke through the weld seam first rather than the window screen itself, although the pressure differential required to do so was equal to the bubble-point pressure. As the test proceeded, and the vapor space volume increased, the pressure differential between the vapor space and the exterior slowly decreased to a value of about 0.2 of the bubble-point pressure, where it then appeared to stabilize. During some of the tests, the draining was halted at intermediate points to verify that the current pressure (vacuum) in the vapor space volume could
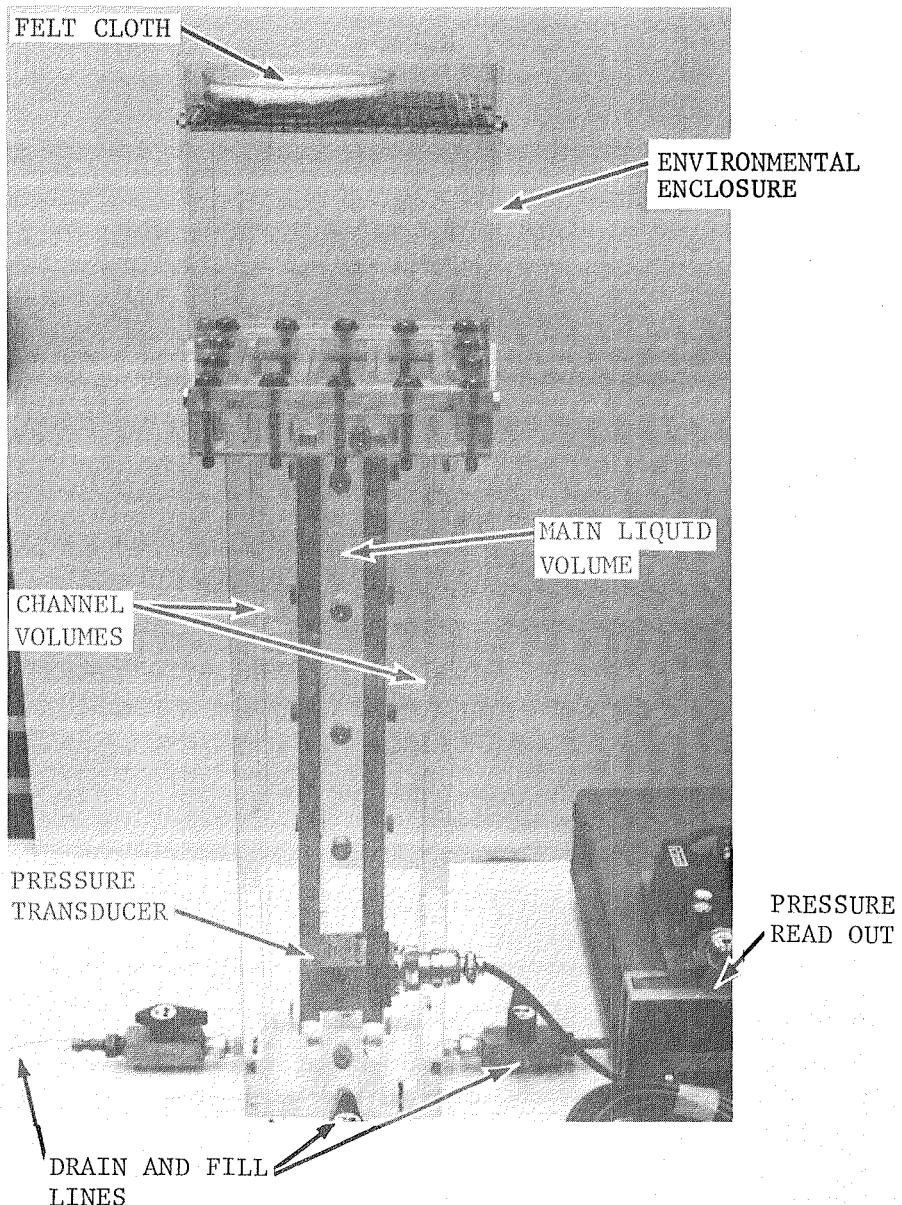
a. Overall View

FIGURE 10. SIMULATED START BASKET
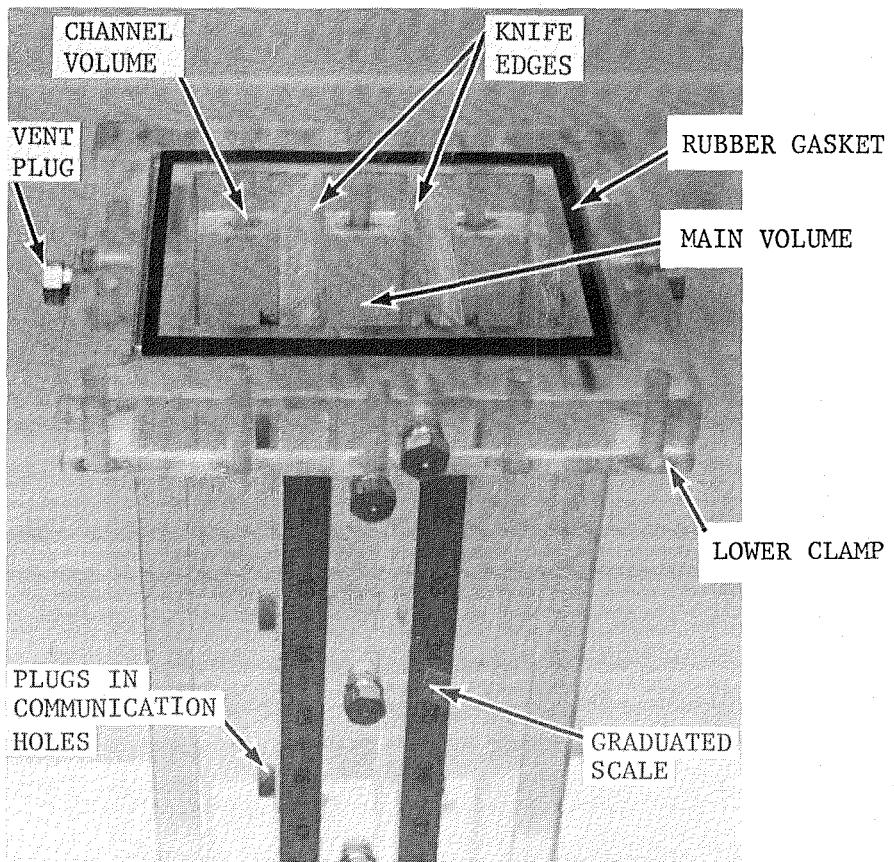
b. Close-up of Screen Area
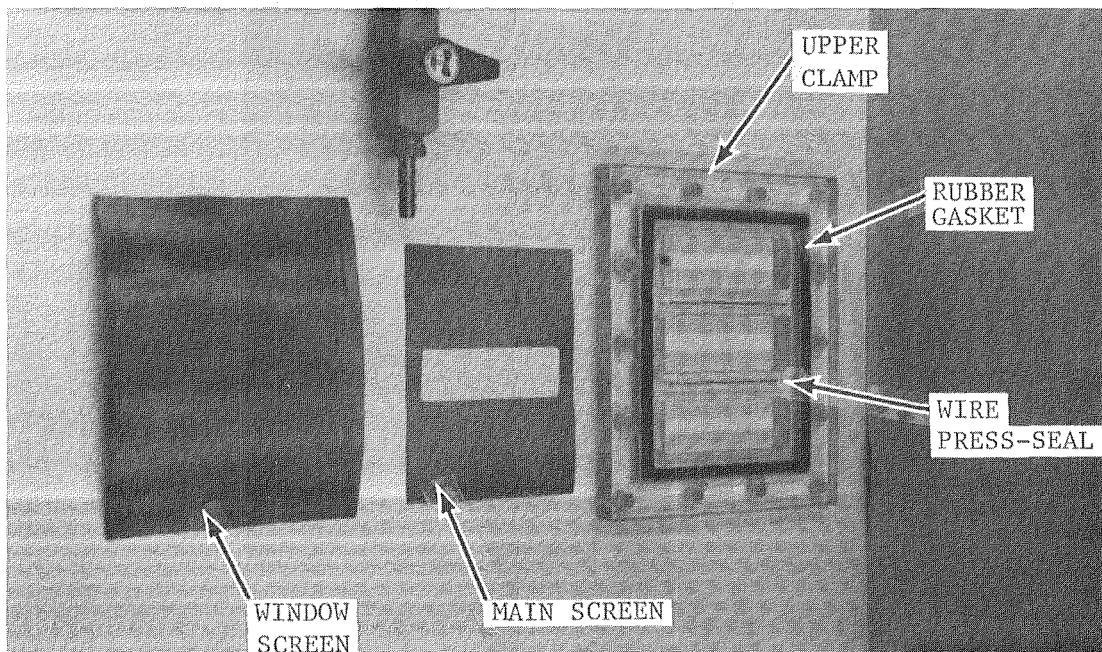
c. Screens and Screen Clamp

FIGURE 10 (Continued). SIMULATED START BASKET

be maintained. This turned out to be the case, thus indicating that the window screen did act as a seal. For any given rate of liquid drainage from the main volume, ΔP_{ov} was a smaller percentage of the window screen bubble-point for isopentane than for ethanol; the importance of internal evaporation was thereby demonstrated. In all the tests, the gravity head h (Figure 1) eventually exceeded the bubble-point of the main screens. Gas then flowed through all the screens, and the liquid level in all three volumes equalized rapidly.

The observed response of the start basket was not anticipated in the light of previous tests where a cyclic inflow was obtained (Ref. 2) or from bubble-point testing (Ref. 10) where the screens were found to re-seal after the imposed pressure differential fell below about fifty-seven percent of the bubble-point. (At this time, the real significance of the decreased pressure in the channel volumes, as expressed in Equation (16) or (25), had not yet been appreciated.) It was decided to repeat the tests using an arrangement that would prevent inflow at the weld seams in the belief that the seams were the source of the unexpected behavior. Several different methods of increasing the tightness of the weld seams were attempted. But even though the normal bubble-point of the screens could be attained, the inflow always broke through first at the seam in all the arrangements, as visual observation showed. It was finally decided to use a double-screen arrangement, as shown in Figure 10c. The main screen was fabricated to fit snugly within the lower rubber gasket and to cover the entrances to all three channels. A central area was cut out as shown to uncover the main volume just inside the knife-edges. A window screen, also large enough to cover all three channel entrances, was laid over the main screen and bolted down with the upper clamp. In this way, the bubble-point of the screen over the main volume remained equal to that of the window screen, while the bubble-point of the channels remained equal to that of the main screens. The screens made intimate contact over the knife edges as well as near the clamping surfaces, and preliminary testing showed that wicking from the channel liquid to the window screen was not impeded.

The test series was then repeated. The results were not markedly different than before. Figures 11 and 12 show measurements from two typical
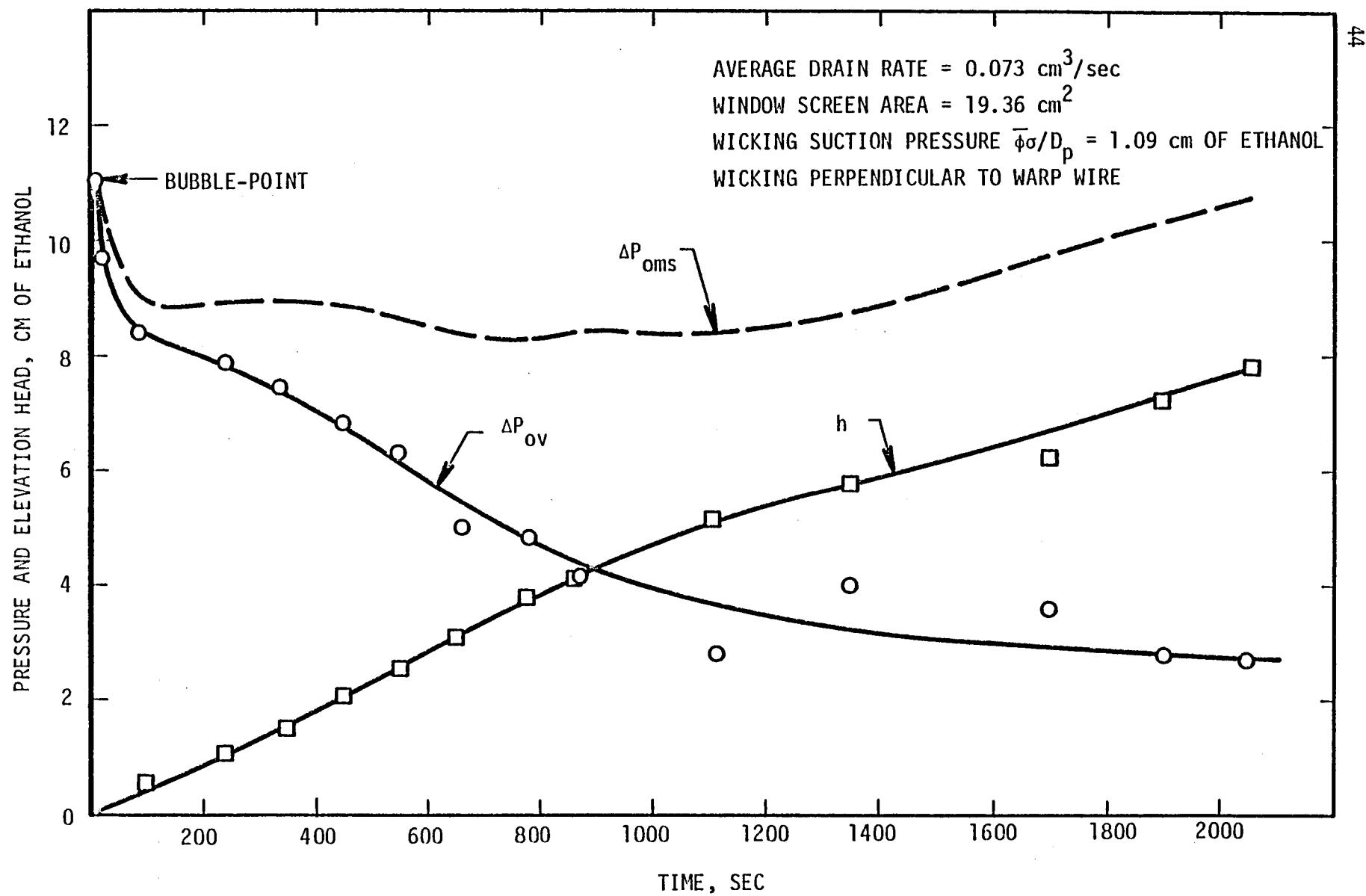
FIGURE 11. RESPONSE OF START BASKET CONTAINING ETHANOL
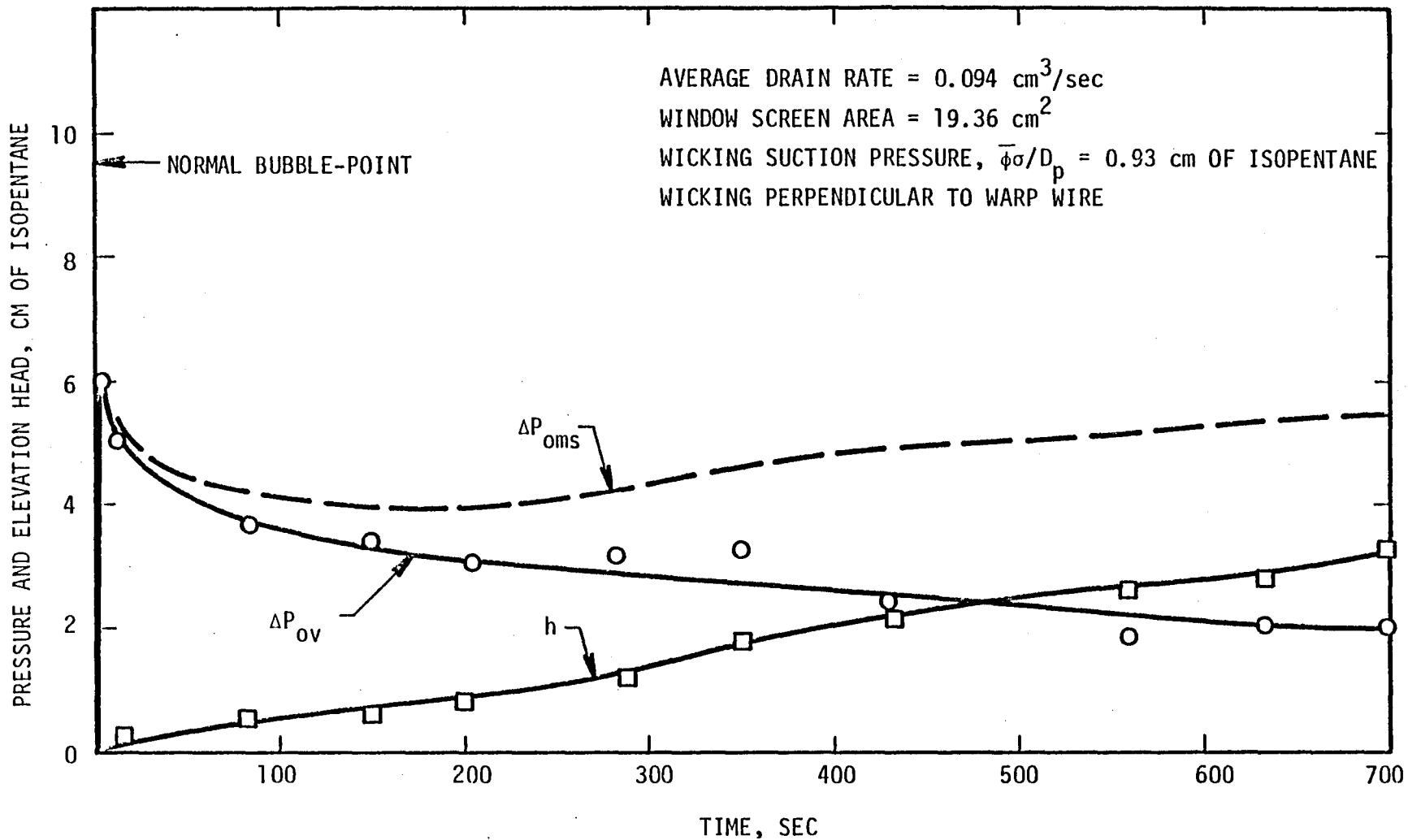
FIGURE 12.   RESPONSE OF START BASKET CONTAINING ISOPENTANE

tests, as well as the computed values of the channel liquid vacuum pressure, $\Delta P_{oms} = \Delta P_{ov} + h$. For both the ethanol and isopentane tests, the window screen appeared to break down initially as a result of ΔP_{ov} exceeding the bubble-point, rather than by drying out as a result of evaporation exceeding the wicking capability of the window screen. The effect of evaporation from the window screen is apparent in the isopentane results, however, since the observed bubble-point was only 63 percent of normal. (From Equation (27) with $K_2 = 0.5$, this corresponds to an evaporation rate equal to 74 percent of the maximum allowable.)

For the ethanol test, ΔP_{ov} gradually decreased to a stabilized value of about 25 percent of the bubble-point. For isopentane, the decrease was more rapid, although the pressure stabilized again at about 25 percent of the normal bubble-point, or 33 percent of the test bubble-point. The long period of nearly constant ΔP_{ov} during the isopentane test demonstrates the influence of internal evaporation. In fact, the vapor space pressure would stabilize at a vacuum head of 3 cm of isopentane entirely as a result of internal evaporation if α in Equation (34) were equal to 0.98, since this value makes the internal evaporation rate equal to the drain rate. Such a value of α is perhaps larger than should be expected, so inflow across the screen is still necessary, although of a smaller magnitude than needed for a similar ethanol test.

Occasionally, a test would be halted during the time when ΔP_{ov} had stabilized, in order to note whether ΔP_{ov} would change. It was found that ΔP_{ov} would decrease by about 0.5 to 1.0 cm of liquid. The change apparently represented the pressure difference required to maintain the inflow. That is, the pressure difference $\Delta P_{ov} - K_4 (\Delta P_{ov})_{max}$ appeared to be about 0.5 - 1.0 cm of liquid, where $(\Delta P_{ov})_{max}$ was the current bubble-point pressure. [$(\Delta P_{ov})_{max}$ at those times must have been considerably less than the normal bubble-point for reasons explained later.)] Using tabulated properties of the screen to compute F_{ws} (Ref. 14), Equation (39) shows that the value of A_f/K_f was on the order of 10^{-4}; this calculation again demonstrates that inflow occurs over only a small fraction of the window screen area.

After further analysis of the data, it was concluded that the unanticipated continuous decrease of ΔP_{ov}, and the absence of cyclic inflow, was a result of the channel liquid vacuum pressure, ΔP_{oms}, exceeding the wicking suction pressure, $\phi\sigma/D_p$, of the window screen. As explained earlier in conjunction with Equation (16), that would lead to a gradual thinning of the liquid layer in the window screen as liquid is withdrawn into the channel. The effect is the same as evaporation from an initially wet screen not in contact with a supply of wicking fluid; as shown in Ref. 10, the bubble-point decreases in such cases. Thus, the decrease in ΔP_{ov} observed in the tests of this study is a consequence of a similar decrease of the window screen bubble-point. The difference between ΔP_{ov} and the actual bubble-point (which clearly could not be measured in these tests) is just sufficient to create a driving pressure difference for the inflow.

To verify the conclusion about thinning of the window screen liquid, several tests were conducted in which small amounts of liquid were periodically added directly to the window screen in order to replenish any liquid withdrawn into the channels. The amounts were sufficient only to wet the screen, and did not form a pool. The vapor space pressure differential was found to increase immediately after adding the liquid, which indicates therefore that the screen had partially dried out. As additional evidence, it was noted during the tests that the window screen lost its "glassy" wet appearance after some time. The screen remained at least partially wet, however, as was verified by touching the screen with tissue paper, which became damp by wicking liquid out of the screen.

The start basket tests reported by others in Ref. 2 are also understandable in terms of the channel liquid vacuum pressure and the resultant thinning of the liquid layer in the window screen. In one configuration, the window screen had a very small surface area (a circle of 0.64 cm diameter) and communicated with a liquid volume of much larger surface area through a 2.5 cm long, 0.64 cm diameter tube. The window screen was attached to the

main screen by an arrangement that allowed a small pool of rewetting liquid to exist in the space between the window screen and main screen. Cycling of the inflow was observed with this configuration until the liquid level had dropped below some critical level. It is concluded that the small size of the window screen and its attachment method to the main screen allowed edge effects to keep the window screen completely wet even though the channel liquid vacuum pressure exceeded the window screen suction pressure. Since the liquid level dropped very slowly (because of the large ratio of liquid surface area to window screen area), the window screen could alternately break down and re-seal for a long period of time with little change in the liquid level. Eventually, however, the negative liquid head in the channel liquid would become large enough to cause the window screen to dry out. Then, the response was similar to that shown in Figure 11 or 12. When larger start baskets with a more extensive window screen were tested, cycling inflow was not observed consistently; in fact, cycling was not observed in most of the tests. During tests of that configuration, the thickness of the liquid layer in the window screen probably decreased as a result of the channel liquid vacuum, analogously to the tests of this study. (The explanations given in Ref. 2 of the observed behavior did not include a consideration of the effects of channel liquid vaccum pressure and do not seem conclusive.)

Note that the ΔP_{ov} trends given in Figures 11 and 12 do not preclude the possibility of cyclic inflows for other test arrangements. If the surface area of the main liquid is much greater than the window screen area, the liquid level h will decrease very slowly for a given drainage rate. Then, at a time when ΔP_{ov} has become smaller than $\phi\sigma/D_p$, ΔP_{oms} would also be less than $\phi\sigma/D_p$, since the static head h would be negligible. The window screen could, consequently, wick liquid from the main screen and re-seal, thus halting the inflow. The initial bubble-point pressure would be re-established, and the cycle would begin again. This would, in fact, be the expected behavior in low-gravity, since there the static head would be much smaller than in ground-based tests.

The overall behavior of the simulated start basket, although initially unexpected, is concluded to be in agreement with the predictions of the

analytical models developed in this study. Unfortunately, quantitative comparisons cannot be made for two reasons:

1. A model is needed to predict the thinning with time of the window screen liquid layer for positive values of $\Delta P_{oms} - \phi_{ws}\sigma/D_{pws}$. The change in the bubble-point as a function of the thinning also must be developed. (Note that Equation (16) predicts a dry-out from the center of the liquid, rather than a thinning, and so is not a suitable model for $\Delta P_{oms} > \phi_{ws}\sigma/D_{pws}$.)

2. Experimental data is needed to quantify the relation between vapor inflow and the pressure difference across a wet window screen.

4. CONCLUSIONS AND RECOMMENDATIONS

An analytical model was developed that prescribes the conditions for vapor flow through the window screen of a capillary acquisition device (start basket). Experiments were conducted to determine the empirical, or correlation, constants used in various parts of the model and to verify the inflow predictions for an idealized start basket.

In addition to the models of wicking flow and bubble-point pressure that have been used in many previous studies, in this study several new sub-models were developed that predict:

1. Decrease in the bubble-point pressure of a screen in the presence of wicking

2. Decrease of the wicking ability of a screen in the presence of a pressure differential across the screen thickness

3. Maximum allowable evaporation rate of liquid from a wicking screen

4. Effective flow thickness of a screen

5. Conditions for the drying out or the vapor penetration of a screen that is simultaneously wicking and resisting a pressure difference

6. Vapor inflow rate as a function of pressure difference across a wet screen

7. Effect on wicking of a difference between the static pressure of the liquid reservoir and the surrounding vapor.

All these relations are needed to assess the performance of a start basket. A large number of separate-effects tests were conducted to verify sub-models (1) through (5) above and to determine the empirical constants appearing in them. It was concluded that the models are successful in quantitatively predicting the correct functional dependence of the important parameters.

The equations of the entire model were solved for typical start-basket designs. The computed results show that:

● Evaporation of liquid into the vapor can control the
response of the start basket under some conditions, by
maintaining an internal pressure sufficient to prevent
the breakdown of the window screen.

● Cycling of the inflow (i.e., alternating periods of inflow
and window screen re-sealing) can occur if the window
screen does not partially dry out because of excessive heat
loads.

● The pressure in the liquid in the channels surrounding the
main liquid volume will decrease as the pressure in the vapor
space decreases, and at some point may exceed the wicking
pressure capability of the window screen, after which the
liquid layer in the screen will thin and the bubble-point
will decrease. When this occurs, the pressure difference
across the window screen can decrease to levels below that
which would normally cause the window-screen to reseal.
Whether cycling of the inflow then occurs is dependent upon
the design of the start basket and the gravity level.

A simplified start basket was constructed and tested to verify these
predictions. Both volatile and non-volatile liquids were used in the
tests. In general, the results verified the trends predicted by the model.
Quantitative comparisons could not be made, however, because of the lack
of adequate measurements needed to evaluate the sub-models described in
(6) and (7) above. The model also explained the observations reported
from other test programs.

A further series of separate-effects tests is recommended to complete
the development of the model. The recommended tests are described as
follows:

1. The relation between the flow rate across a wet screen, the
imposed pressure difference, and the screen bubble-point

should be quantified. Such tests might be conducted with a bubble-point apparatus modified to permit wicking without using a standing pool of liquid on the screen. After imposing a pressure differential greater than the bubble-point (to cause the screen to breakdown) the pressure differential should be maintained at various levels greater than the resealing pressure but less than the bubble-point. The resulting gas flow rates should be measured.

2.   The effect of decreasing the liquid reservoir pressure on the ability of a screen to wick should be verified. Such tests could be conducted with a horizontal wicking apparatus, similar to that used in this study, but modified to allow the reservoir static head to be decreased. (A sealed reservoir would be required.) By correlating the wicking distance with wicking time (or wicking velocity with wicking length), the ratio of the wicking resistance with and without an imposed reservoir vacuum pressure could be determined. Alternatively, a vertical wicking apparatus could be modified similarly to determine $\phi\sigma/D_p - \Delta P_{reservoir}$ directly.

3.   The rate of liquid layer thinning and the effect on the bubble-point should be determined. For these tests, a bubble-point apparatus could be modified as in (1) above so that the screen has a source of wicking liquid. The static head of the reservoir would be maintained at various constant vacuum levels and the decrease in the bubble-point pressure of the screen measured as a function of time. It would also be valuable to determine the rate of thinning by measuring the volume of liquid withdrawn from the screen into the reservoir.

With the results of these recommended tests, the analytical model of vapor inflow into start baskets can be quantified for all conditions of interest.

5. REFERENCES

1. The Dynamic Behavior of Liquids in Moving Containers, ed. H. N. Abramson, Chapter 11, NASA SP-106, 1966 (Reprinted by Southwest Research Institute, 1981.)

2. M. H. Blatt and J. A. Risberg, "Study of Liquid and Vapor Flow into a Centaur Capillary Device," Report GDC-NAS-79-001 (NASA CR-159657), General Dynamics/Convair, 1979.

3. M. H. Blatt and M. D. Walter, "Centaur Propellant Acquisition System Study," Report CASD-NAS-75-023 (NASA CR-134811), General Dynamics/ Convair, 1975.

4. E. C. Cady, "Effect of Transient Liquid Flow on Retention Characteristics of Screen Acquisition Systems," Report MDC G6742 (NASA CR-135218), McDonnell Douglas Astronautics, 1977.

5. P. E. Bingham and J. R. Tegart, "Wicking in Fine Mesh Screens," AIAA Paper 77-849, AIAA/SAE 13th Propulsion Conference, July 1977.

6. J. C. Armour and J. N. Cannon, "Fluid Flow Through Woven Screens," AIChE J., Vol. 14, May 1968, pp 415-420.

7. R. T. Bernardi, J. H. Lineham, and L. H. Hamilton, "Low Reynolds Number Loss Coefficients for Fine-Mesh Screens," Trans. ASME, J. Fluids Engrg., Vol. 98, Dec. 1976, pp 762-763.

8. E. P. Symons, "Wicking of Liquids in Screens," NASA TN D-7657, May 1974.

9. E. D. Simon, "Environmental Requirements for Bubble Pressure Tests on Fine-Mesh Screens," AIAA J. Spacecraft and Rockets, Vol. 16, July-August 1979, pp 218-222.

10. H. L. Paynter, " Acquisition/Expulsion System for Earth Orbital Propulsion System, Volume III, Cryogenic Test," Report MCR-73-97, Martin Marietta Corp., Oct. 1973.

11. J. P. Hirth and G. M. Pound, Condensation and Evaporation Growth Kinetics, MacMillan Co., 1963.

12. Chemical Engineers' Handbook, ed. J. H. Perry, 4th edition, p 4-48, McGraw-Hill Book Co., 1963.

13. T. Boublik, V. Fried, and E. Hala, The Vapour Pressure of Pure Substances, Elsevier Scientific Publishing Co., 1973.

14. Anon, "Low Gravity Propellant Control Using Capillary Devices in Large Scale Cryogenic Vehicles. Design Handbook," Report GDC-DDB70-066, General Dynamics/Convair, 1970.

APPENDIX

LIST OF SYMBOLS

LIST OF SYMBOLS

Note: The subscript "ms" or "ws" added to any of the symbols indicates that the parameter is evaluated for the main screen or the window screen, respectively.

a	empirical coefficient in screen flow-through equation (dimensionless)
A_f	fraction of screen area open to flow (dimensionless)
A_i	interfacial area between main liquid volume and vapor
A_o	outer surface area of start basket exposed to heat
A_{vs}	surface area (screen plus liquid) of vapor space
A_{wet}	area of inner main wcreens wet on both sides
b	screen thickness
b_f	effective thickness of screen open to wicking
B	window screen width normal to wicking velocity
C	screen wicking resistance (dimensionless)
C_p	specific heat of liquid
D_p	bubble-point diameter
F	screen flow-through resistance factor (dimensionless) equal to bA_r^2Q/V_r^2, where b = screen thickness, A_r = screen surface area/volume, Q = tortuosity factor, and V_r = void volume/screen volume
F_j	Concentrated flow resistance of window-screen/main screen junction
g	gravity
h	distance to liquid surface below window screen
h_{f_g}	heat of vaporization of liquid
H	total height of start basket
K_1, K_2, K_3, K_4	empirical factors, see equations (17), (26), (33), and (39)
K_f	vapor flow-through resistance ratio of wet to dry screen

ℓ	wetted or wicking length of window screen
L	half-length of window screen
$\dot{m}_e$	internal liquid evaporation rate per unit area
$\dot{m}_0$	external liquid evaporation rate per unit area
$\dot{m}_s$	flow across main screen from main liquid volume to channel volume per unit area
$\dot{m}_w$	evaporation rate from window screen per unit area
$\dot{M}_v$	vapor flow across window screen
P	vapor space pressure
P_c	channel liquid pressure
$P_{c\ell}, P_{cu}$	channel liquid pressure at bottom and top of basket
P_ℓ	main liquid pressure at bottom of basket
P_L	main liquid pressure
P_0	external vapor pressure
P_{sat}	liquid saturation pressure
P_w	pressure in wicking liquid
P_σ	wicking suction pressure
$\Delta P_{\ell v}$	$P_{sat} - P$
ΔP_{ov}	$P_0 - P$
ΔP_{oms}	$P_0 - P_{cu}$
ΔP_w	wicking pressure difference from end-to-end of screen induced by capillarity
$\dot{q}$	heat flux impinging on external screens
R	gas constant of vapor
t	time
T	liquid temperature
v_w	wicking velocity

V	vapor space volume
V_L	main liquid volume
α	empirical constant for internal evaporation, Eq. (34)
μ_L, μ_0	viscosity of liquid and vapor
ρ_L	liquid density
$\phi, \bar{\phi}$	capillary wicking constant with and without an imposed pressure differential across screen

CONTRACT NAS3-22664
REPORT DISTRIBUTION LIST

Name   No. of Copies

National Aeronautics & Space Administration
Lewis Research Center
21000 Brookpark Road
Cleveland, OH 44135

Attn: Communications & Propulsion Section, MS 500-306   1
       E. A. Bourke, MS 501-5   2
       Technical Utilization Office, MS 3-19   1
       Technical Report Control Office, MS 5-5   1
       AFSC Liaison Officer, MS 501-3   2
       Library, MS 60-3   2
       Office of Reliability & Quality
         Assurance, MS 500-211   1
       E. P. Symons, Project Manager, MS 501-6   40
       L. J. Ross, MS 3-7   1
       D. A. Petrash, MS 501-5   1
       R. J. Priem, MS 501-6   1
       T. H. Cochran, MS 501-7   1
       S. H. Gorland, MS 501-8   1
       G. R. Smolak, MS 501-6   1
       J. C. Aydelott, MS 501-6   1
       T. L. Labus, MS 501-7   1

National Aeronautics & Space Administration
Headquarters
Washington, D. C. 20546

Attn: RS-5/Director, Space Systems Division   1
       RT-6/Director, Research & Technology Division   1
       RTP-6/F. W. Stephenson   1
       MHE-7/P. N. Herr   1
       RST-5/E. Gabris   1
       RST-5/M. Cuviello   1

National Aeronautics & Space Administration
Goddard Space Flight Center
Greenbelt, MD 20771

Attn: Library   1
       A. Sherman, MS 713   1

National Aeronautics & Space Administration
John F. Kennedy Space Center
Kennedy Space Center, FL 32899

Attn:	Library	1
	DD-MED-41/F. S. Howard	1
	DF-PED/W. H. Boggs	1

National Aeronautics & Space Adminstration
Ames Research Center
Moffett Field, CA 94035

Attn:	Library	1
	J. Vorreiter, MS 244-7	1
	Dr. W. Brooks, MS 244-7	1

National Aeronautics & Space Administration
Langley Research Center
Hampton, VA 23365

| Attn: | Library | 1 |

National Aeronautics & Space Administration
Johnson Space Center
Houston, TX 77001

Attn:	Library	1
	EP2/Z. D. Kirkland	1
	EP5/W. Chandler	1
	EP4/Dale Connelly	1
	ED4/C. J. LeBlanc	1

National Aeronautics & Space Administration
George C. Marshall Space Flight Center
Huntsville, AL 35812

Attn:	Library	1
	EP43/L. Hastings	1
	EP43/A. L. Worlund	1
	EP41/Dr. Wayne Littles	1
	EP24/G. M. Chandler	1
	ES63/E. W. Urban	1

Jet Propulsion Laboratory
4800 Oak Grove Drive
Pasadena, CA 91103

Attn: Library   1
       Don Young, MS 507-228   1
       T. Oslander   1

NASA Scientific & Technical Information Facility
P. O. Box 8757
Balt./Wash. International Airport, MD 21240

Attn: Accessioning Department   10

Defense Documentation Center
Cameron Station - Bldg. 5
5010 Duke Street
Alexandria, VA 22314

Attn: TISIA   1

National Aeronautics & Space Administration
Flight Research Center
P. O. Box 273
Edwards, CA 93523

Attn: Library   1

Air Force Rocket Propulsion Laboratory
Edwards, CA 93523

Attn: LKCC/J. E. Brannigan   1
       LKDS/R. L. Wiswell   1
       LKDM/Wayne Pritz   1
       LKCC/R. A. Silver   1

Aeronautical Systems Division
Air Force Systems Command
Wright Patterson Air Force Base
Dayton, OH 45433

Attn: Library   1

Air Force Office of Scientific Research
Washington, D. C. 20333

Attn: Library   1

Aerospace Corporation
2400 E. El Segundo Blvd.
Los Angeles, CA 90045

Attn: Library - Documents   1

Beech Aircraft Corporation
Boulder Facility
Box 9631
Boulder, CO 80301

Attn: Library   1
       R. A. Mohling   1
       S. Willen   1

Bell Aerosystem, Inc.
Box 1
Buffalo, NY 14240

Attn: Library   1
       J. Colt   1
       T. Hinterman   1

Boeing Company
P. O. Box 3999
Seattle, WA 98124

Attn: Library   1
       C. L. Wilkensen, MS 8K/31   1

Chrysler Corporation
Space Division
P. O. Box 29200
New Orleans, LA 70129

Attn: Library   1

McDonnell Douglas Astronautics Co.
5301 Balsa Avenue
Huntington Beach, CA   92647

Attn: Library   1

General Dynamics Corp./Convair Division
5001 Kearny Villa Road
San Diego, CA   92138

Attn: Library   1
       R. Bradshaw   1
       D. Heald   1

Missiles and Space Systems Center
General Electric Company
Valley Forge Space Technology Center
P. O. Box 8555
Philadelphia, PA   19101

Attn: Library   1

IIT Research Institute
Technology Center
Chicago, IL   60616

Attn: Library   1

Lockheed Missiles & Space Company
P. O. Box 504
Sunnyvale, CA   94087

Attn: Library   1
       G. D. Bizzell   1
       S. G. DeBrock   1

Battelle Memorial Institute
Columbus Labs
505 King Avenue
Columbus, Ohio   43201

Attn: E. Rice   1

Space Division
Rockwell International Corp.
12214 Lakewood Blvd.
Downey, CA 90241

Attn: Library   1
       A. Jones   1

Northrop Research & Technology Center
1 Research Park
Palos Verdes Peninsula, CA 90274

Attn: Library   1

TRW Systems, Inc.
1 Space Park
Redondo Beach, CA 90278

Attn: Tech. Lib. Doc. Acquisitions   1

National Science Foundation, Engr. Div.
1800 G. Street, NW
Washington, D. C. 20540

Attn: Library   1

Florida Institute of Technology
M. E. Department
Melbourne, FL 32901

Attn: Dr. T. E. Bowmann   1

RCA/AED
P. O. Box 800
Princeton, NJ 08540

Attn: Mr. Daniel Balzer   1

Martin Marietta
Denver Aerospace
P. O. Box 179
Denver, CO 80201

Attn: D. A. Fester   1
       R. N. Eberhardt   1
       J. Tegart   1

McDonnell Douglas Astronautics Co.-East
P. O. Box 516
St. Louis, MO 63166

Attn: G. Orton   1
       W. Regnier   1

Science Applications, Inc.
1200 Prospect Street
P. O. Box 2351
La Jolla, CA 92037

Attn: M. Blatt   1

Xerox Electro-Optical Systems
300 North Halstead
Pasadena, CA 91107

Attn: Robert Richter   1

End of Document